



HAL
open science

Seasonal types in homogeneous rainfall regions of the Amazon basin

Véronique Michot, Thomas Corpetti, Josyane Ronchail, Jhan Carlo Espinoza, Damien Arvor, Beatriz M Funatsu, Vincent Dubreuil

► **To cite this version:**

Véronique Michot, Thomas Corpetti, Josyane Ronchail, Jhan Carlo Espinoza, Damien Arvor, et al.. Seasonal types in homogeneous rainfall regions of the Amazon basin. *International Journal of Climatology*, 2024, 44 (4), pp.1224-1244. 10.1002/joc.8380 . halshs-04476362v2

HAL Id: halshs-04476362

<https://shs.hal.science/halshs-04476362v2>

Submitted on 8 Nov 2024

HAL is a multi-disciplinary open access archive for the deposit and dissemination of scientific research documents, whether they are published or not. The documents may come from teaching and research institutions in France or abroad, or from public or private research centers.

L'archive ouverte pluridisciplinaire **HAL**, est destinée au dépôt et à la diffusion de documents scientifiques de niveau recherche, publiés ou non, émanant des établissements d'enseignement et de recherche français ou étrangers, des laboratoires publics ou privés.



Distributed under a Creative Commons Attribution - NonCommercial - NoDerivatives 4.0 International License

RESEARCH ARTICLE

Seasonal types in homogeneous rainfall regions of the Amazon basin

Véronique Michot^{1,2}  | Thomas Corpetti² | Josyane Ronchail³ |
 Jhan Carlo Espinoza^{4,5}  | Damien Arvor² | Beatriz M. Funatsu² |
 Vincent Dubreuil² 

¹Université Paris Cité, UMR 8586
 PRODIG, Paris, France

²Université Rennes 2, CNRS, Nantes
 Université, LETG, UMR 6554, Rennes,
 France

³Laboratoire d'Océanographie et du
 Climat, LOCEAN-IPSL, Sorbonne
 Université, IRD, CNRS, MNHN, Paris,
 France

⁴Université Grenoble Alpes, IRD, CNRS,
 Grenoble INP, Institut des Géosciences de
 l'Environnement (IGE, UMR 5001),
 Grenoble, France

⁵Instituto de Investigación sobre la
 Enseñanza de las Matemáticas,
 Universidad Católica del Perú, (PUCP),
 Lima, Peru

Correspondence

Véronique Michot, Université Paris Cité,
 UMR 8586 PRODIG, 75013 Paris, France.
 Email: veronique.michot@u-paris.fr

Funding information

Université de Rennes 2

Abstract

Due to its size and geographical features, different average annual rainfall regimes co-exist in the Amazon basin, with distinct year-to-year variability dependent on regions within the basin. In this study, we define and explain the seasonal regional types of annual regimes, that is, years with similar seasonal anomalies. Our work is based on a 205 rain gauge network distributed over five Amazonian countries, spanning a period over 30 years. Using a spectral clustering method, we identified seven sub-regions within the basin in which annual rainfall regimes are spatially homogenous. For each sub-domain, we estimated specific parameters that characterize the rainy season (onset and demise dates, sign and duration of rainfall anomalies). Finally, using spectral analysis we identified between two and four 'seasonal type' of precipitation in these seven sub-domains. Most of these seasonal types are in phase with the large-scale atmospheric circulation, which explains the temporal link with rainfall anomalies. The seasonal types result of the superposition of inter-annual and intra-seasonal variability whose factors are then difficult to identify and attribute. Part of the rainfall anomalies characterizing seasonal types is related to the inter-annual variability of the sea surface temperature in the Atlantic or the Pacific oceans, especially in the northeast and southeast part of the Amazon basin, whereas in other parts, strong intra-seasonal and local factors have a larger impact. The same sign and duration of anomalies do not concomitantly affect the various regions of the Amazon basin, confirming that one mode of variability does not homogeneously affect precipitation in different parts of the basin.

KEYWORDS

precipitation regimes, rain gauge network, sea surface temperature, seasonal type, spectral clustering

1 | INTRODUCTION

The Amazon basin (AB) is very often reduced to the mere image of evergreen forest continuously showered with

large amounts of rain. However, the diversity of environments and precipitation regimes are complex and stems in particular from the size of the Amazonian watershed, which extends from the Andes to the Atlantic covering

more than 6 million km². Located in the intertropical zone between 5° N and 20° S, the AB regional climate is regulated by the South American monsoon, the displacement of the Intertropical convergence zone (ITCZ) and on their seasonality (Vera, Baez, et al., 2006; Vera, Higgins, et al., 2006). Average precipitation and rainfall regimes are highly contrasted (see, e.g., Espinoza Villar et al., 2009; Figueroa & Nobre, 1990; Marengo, 1992; among others). According to the Köppen climate classification, the basin falls within a type A warm climate, with subtypes Af (tropical wet without a dry season) in the west and along the Negro River and Am (tropical monsoon) and Aw (tropical savanna with dry winter) in the north, northeast, south and southeast. In the equatorial Amazon–Andes transition zone, several seasonal rainfall regimes are identified in few kilometres due to the interaction between regional atmospheric circulation and the Andean topography (Espinoza et al., 2009; Laraque et al., 2007; Segura et al., 2019). Between 50% and 70% of rainfall in the AB comes from the Atlantic via moisture advection, variable according to the season, through the ITCZ (Arraut and Satyamurty 2009; 2012; Costa and Foley 1998; Durieux 2002; Satyamurty et al., 2013; Wang & Fu, 2002). Moisture flows enter the basin mainly to the east at around 45° W and to the north. Convective systems are able to reach the Andes thanks to contribution of synoptic circulation and evapotranspiration from the Amazon rainforest (Segura et al., 2020; Simões Reibota et al. 2010). The Amazon rainforest feeds the atmosphere with moisture through evapotranspiration, and it is estimated that between 33% and 56% of precipitation comes from evapotranspiration (Makarieva et al. 2007; Marques et al. 1977; Molion 1975; Rocha et al. 2015; Salati et al. 1978; Satyamurty et al., 2013). However, southern and southwestern Amazonia differ, with a greater contribution from local recycling by vegetation in the former region than in the latter, which in turn depends on evapotranspiration in other parts of the basin (Staal et al., 2018). Some of the moisture in the AB is also transported southwards towards the sub-tropical regions of southern South America via the low-level jet (LLJ) east of the Andes (Arraut and Satyamurty 2009; Salio et al. 2002) and then is also a source of moisture for the Plata basin. The seasonal precipitation regimes in the AB are, however, highly variable from 1 year to another when compared with the historical mean seasonal regime. Therefore, a high variability in the different parameters of the rainy season can be observed, for instance, in its duration and the onset and demise of the rainiest period, the occurrence of dry spells or in the intensity of intra-seasonal rainfall (e.g., Arvor et al., 2017; Funatsu et al., 2021; Moron et al., 2013).

On an inter-annual time scale, rainfall variability is strongly related to the ocean–atmosphere coupling

modulated by anomalies of the sea surface temperatures (SST). The oceanic phenomenon most often implicated in South American precipitation variability is the El Niño (EN) Southern Oscillation (ENSO) in the Pacific, in which cold [La Niña (LN)] or warm (EN) phases result in rainfall excesses or deficits, depending on the region of the subcontinent (Aceituno, 1988; Kousky et al., 1984; Marengo, 1992; Marengo & Espinoza, 2016; Sulca et al., 2017; Towner et al., 2020, among others). However, the impact of ENSO is variable and depends on its duration, intensity, location in the eastern or central Pacific (Andreoli et al., 2016; Jimenez et al., 2021; Takahashi et al., 2011; Tedeschi et al., 2016) and its association with temperature anomalies in the tropical North and/or South Atlantic. In addition, the role of the Atlantic on the South American rainfall is increasingly highlighted. Indeed, the warming of the tropical North Atlantic is related to a lengthening of the dry season in southern Amazonia and to severe droughts in 2005 and 2010 in the AB (Arias et al., 2020; Marengo et al., 2008; Marengo & Espinoza, 2016; Zeng et al., 2008). Moreover, Espinoza et al. (2014) showed that the exceptional flood of 2014 in the southwestern AB was due to warm conditions in the Indo–Pacific Ocean and a strong warm gradient between the tropical and sub-tropical South Atlantic Ocean.

However, at higher frequency, other atmospheric modes than ENSO or coupling with Atlantic SST anomalies can cause strong precipitation variability. For instance, Mayta et al. (2019) showed that around 25% of the intra-seasonal rainfall extremes in the AB are related to the eastwards propagating equatorially confined Madden–Julian Oscillation (MJO; Madden & Julian, 1971). Other high-frequency mechanisms such as Rossby wave trains in the Southern Hemisphere have been proposed to explain the observed intra-seasonal and synoptic rainfall variability. According to these results, extra-tropical wind intrusions into the southern Amazon and cross-equatorial wind regimes contribute to the weather patterns variability over the AB and associated rainfall (Paccini et al., 2018; Wang & Fu, 2002), including the onset and demise of the wet season in southern Amazon (Arias et al., 2015; Espinoza et al., 2021; Fu et al., 2013).

Several previous studies have focused on rainfall patterns, their spatial and temporal diversity in the AB and their link with SST anomalies, or with the high-frequency phenomena described above, most often with an emphasis on the study of extreme events. However, few studies have been dedicated to analysing systematically the intra-seasonal regional consistency of precipitation anomalies based on long-term in-situ rainfall stations.

The present work contributes to the analysis of intra-seasonal precipitation variability. To this end, we define a ‘seasonal type’ that is cluster of years with similar

intra-seasonal rainfall variability in a regional scale. Furthermore, we aim at explaining the modulation of these seasonal types through the comparison of rainfall anomalies with those of (i) cloud cover, in order to better identify the major convection regions, (ii) the integrated water vapour (IWV) flux circulation which favour or restrict precipitation, and (iii) SST, especially in the tropical and sub-tropical Pacific and Atlantic oceans.

The paper is organized as follows: The Section 2 presents the data used in this study. Section 3 introduces the methods used to distinguish first, homogeneous precipitation regions, then, seasonal types and relate the latter to elements of atmospheric circulation and Pacific and Atlantic SST. Finally, Section 4 presents the results and discusses them before a final section with conclusion and final remarks.

2 | DATA

2.1 | Daily rain gauge data

Rainfall stations offer long (more than 30 years) and relatively reliable time series making it possible to analyse the temporal variability of rainfall on a small scale, despite their sparseness in the AB and possible measurement errors. Rainfall from models derived satellite data also have limitations; the time series rarely cover three decades, and although progress has been made since the first generation satellite (Fassoni-Andrade et al., 2021), rainfall estimates are still difficult to calibrate. Indeed,

rainfall estimations from satellite models often tend to be overestimated. As a matter of fact, even a satellite product from Tropical Rainfall Measurement Mission (TRMM) 3B42, which has one of the longest estimated series and among the best quality, tend to overestimate the mean annual precipitation (Michot et al., 2018) and overestimate precipitations particularly during the rainiest season in south, north and northeast of the AB (Michot et al., 2018) and in west and centre regions during dry season (Michot et al., 2018; Zubieta et al., 2015; Zulkafli et al., 2014). Another major issue for this work is that it is not very reliable to entirely reproduce the seasonal differences of some regions of the AB like in the Marañón and the Ucayali sub-catchments. For this reason, we chose to use observed data, from a network of 205 rain gauges (Figure 1) at daily scale, for which advanced quality control has been implemented (more details can be found in Michot et al., 2019). The data from the stations cover the period from 1981 to 2013 and were obtained from the National Water Agency (ANA) and the National Meteorological Institute (INMET) in Brazil, the National Meteorological and Hydrological Institute (INAMHI) in Ecuador, the Hydrological Meteorological and Environmental Studies Institute (IDEAM) in Colombia, and the respective National Meteorological and Hydrological Services (SENAMHI) in Peru and Bolivia. Unfortunately, no such data could be collected in Venezuela, and in the southwest part of the AB (between 10° S–15° S and 76° W–69° W) because data from stations in these regions did not meet the criteria for the database used for this work (more details can be found in

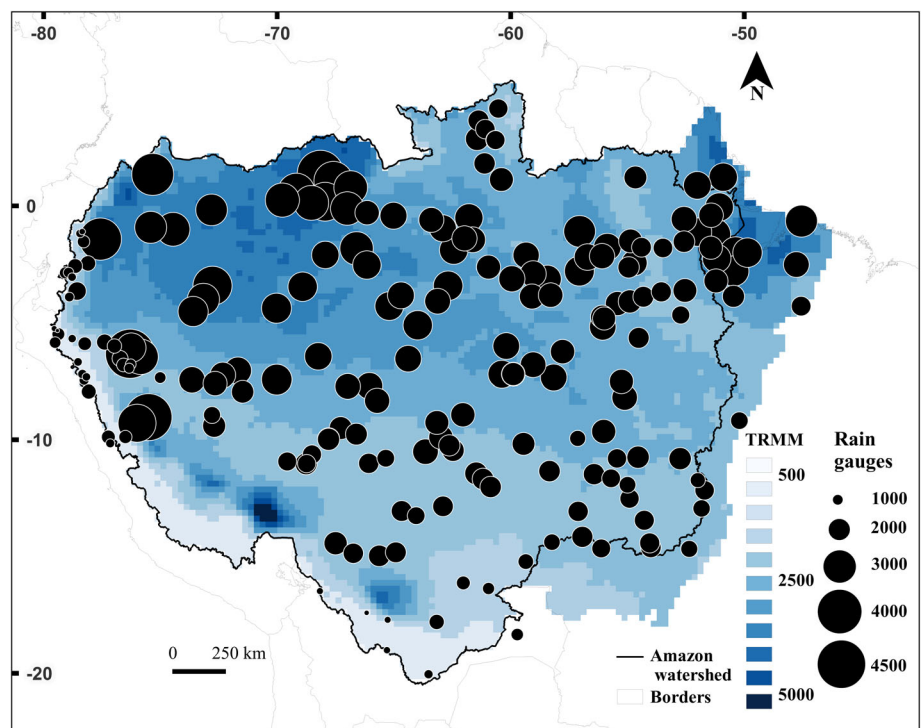


FIGURE 1 Annual mean rainfall in millimetres for the Amazon basin from TRMM B42 v7 (1998–2013) in blue and from network rain gauges (1981–2013) represented by the proportional circles. TRMM, Tropical Rainfall Measurement Mission.

Michot et al., 2019). The rain gauge-based data is able to account for the diversity of mean annual rainfall even though it misses the rainfall hotspots in the south and southwest of the Amazon–Andes transition zone (Chavez & Takahashi, 2017; Espinoza et al., 2015), as shown by the data from the TRMM satellite product (Figure 1).

2.2 | Outgoing longwave radiation and IWV flux

Outgoing longwave radiation (OLR) was used as a proxy of deep convective clouds and was obtained from the National Center for Atmospheric Research of the National Ocean and Atmospheric Administration (NCAR/NOAA; Liebmann & Smith, 1996). IWV reanalysis (Kalnay et al., 1996) that can provide indications about the pressure fields is from the National Center for Environmental Prediction (NCEP–NCAR). The IWV is computed from the specific humidity and the horizontal wind (zonal– u) and meridional (v) from the ground to 300 hPa (Peixoto & Oort, 1992; Satyamurty et al., 2013) as follows:

$$F_W = \int qVp/g, \quad (1)$$

where q is the humidity, V is the wind vector, p is the pressure and g is the acceleration due to gravity. This is a vertically integrated value indicates whether atmospheric motions act to decrease (for divergence) or increase (for convergence) the vertical integral of moisture, over a given time period. High positive values of this parameter (i.e., large moisture convergence) can be related to precipitation intensification and floods.

2.3 | Sea surface temperature data

The NOAA–CPC global monthly SST data at $2 \times 2^\circ$ horizontal grid resolution (Smith & Reynolds, 2004) are used to analyse the variability of surface temperatures in the tropical Pacific and Atlantic oceans. The types of EN and LN events to which we refer to describe the relation between rainfall and oceanic anomalies are detailed in Andreoli et al. (2016), Pillai et al. (2021), Takahashi et al. (2011) and Tedeschi et al. (2016).

3 | METHODS

3.1 | The spectral clustering method

The spectral clustering method is used in order to (i) classify the stations according to their annual regime

and define homogeneous rainfall regime regions in the AB and (ii) classify the years within a region to detect the seasonal types.

The main principle of spectral clustering is to represent all rain gauges in separate nodes of a connected graph whose vertexes express the similarity between two nodes. The spectral analysis of this graph (i.e., analysis of the matrices that represent connections inside the graph) enables it to isolate its main consistent groups. To compute the connection between two nodes into this graph, the basic solution consists in computing the usual Euclidean distance. However, for clusters where the separation is tricky and non-linear, we exploit the kernel trick. It consists in projecting data in a space other than the usual one (i.e., represented by time series of rainfall) where the separation between clusters is linear. Under some specific properties (see Camps-Valls & Bruzzone, 2009 for a complete theory of kernels), this projection can simply be done by changing the way one computes the connection between nodes. In practice, this is done using a Gaussian kernel where the connection between two rain gauges x_1 and x_2 is given by:

$$K(x_1, x_2) = e^{-\frac{\|x_1 - x_2\|^2}{\sigma^2}}, \quad (2)$$

where σ is a parameter to fix. This kernel enables to efficiently separate highly non-linear clusters. By a non-linear separation, we refer to the idea that the boundaries that separate different clusters of rain gauges are not linear in nature. Unlike linear separation, which assumes that clusters can be divided by straight lines or hyperplanes, non-linear separation acknowledges that clusters might be intertwined or have complex, curvy or irregular boundaries that cannot be accurately represented by linear models. Non-linear separation is particularly important when dealing with data in high-dimensional spaces (as in our situation), where linear boundaries may not adequately capture the underlying cluster structure. The non-linear spectral clustering technique aims to uncover hidden patterns and structures of precipitations in the data, even when they are not easily distinguishable by simple linear separation.

3.2 | Determination of homogeneous regions based on their rainfall regimes

Mean historical precipitation regimes are often computed based on a multi-decadal time series, but spatially averaging these series do not discriminate well between homogeneous and transition areas where regimes are less well individualized. Indeed, some regions may have the same year-to-year variability of the seasonal regime and thus

have a stronger spatial consistency, whereas in other regions, the regime is more variable from 1 year to another. Our approach therefore aims to identify the areas where regimes are similar year after year. In order to do this, we first use the spectral clustering method to describe year by year the spatial distribution of rainfall regimes, from August to July of the following year, as most of the rainy seasons or wetter periods are centred on the austral summer. The geographical coordinates of the stations are not considered to avoid forcing spatial homogeneity. Indeed, even if spatial coordinates can be valuable in a clustering problem involving spatial data, in this particular situation where the goal is to obtain homogeneous groups of precipitation whatever the location, it is preferable not to use spatial coordinates to avoid introducing a bias that might cluster nearby stations together. This procedure leads to one classification per year. An open issue of data clustering for which no sound solution yet exists is the determination of the optimal number of clusters. In this study, we rely on the intra/inter inertia to obtain reliable clusters. A good clustering should indeed exhibit homogeneous data within each cluster and a large variability between different clusters (e.g., between the mean of each cluster). This notion of homogeneity can be quantified using the standard deviation of the data: the average of the standard deviations of the time series within each cluster gives the intra-class variance and the standard deviation between the centres of each cluster gives inter-class variance. Therefore, the ratio between the inertia among clusters and the internal inertia should be maximal. Applying this approach to each year of the series, the optimal number of clusters obtained is 13 per year. Small clusters (less than five rain gauges) are gathered with the nearest cluster (considering the spatial distance and inter-class variance); in this case, the number of annual clusters is reduced 10 to 6.

Finally, to analyse the pairing of the stations, that is, to define which stations were most often part of the same cluster, we mapped the weight of the link between the stations through the time series thanks to the ‘Cartography’ package of the R-cran software (<http://rgeomatic.hypotheses.org/659>). This allowed us to visualize the sectors within which the annual regimes were most often similar. Conversely, stations with more random behaviour were determined as belonging to a transition region.

3.3 | Detection of seasonal type in a homogeneous region

Since the inter-annual variability of daily precipitation is very high, the intercomparison of annual patterns was

achieved by performing a Fourier transform to smooth the data, removing frequencies higher than 60 days. On the one hand, this frequency allows to observe, if it is the case, alternating rainfall anomalies during the season, whereas higher frequencies show only one anomaly direction. On the other hand, this time step may correspond to intra-seasonal atmospheric variability modes. Thus, a smoothing of 60 days allowed us to keep a daily time step with a reduced noise so that we could observe more adequately the evolution of the annual regime of precipitation.

From these smoothed annual regimes, we identified in each region the clusters of years that have had a similar rainfall regime, which correspond to our seasonal types, using the previously described spectral clustering method. The maximum number of seasonal types is arbitrarily set at four but without imposing any minimum number. The years are as before, defined from August to July of the following year, with the exception of the northern region where the rainy season is aligned to the boreal summer (Rao & Hada, 1990), that is, from June to September. The number of years within these seasonal types is very heterogeneous; a greater homogeneity between them is obtained by eliminating the least representative years in each type. Years are eliminated when their distance from the mean regime is greater than a threshold, which is the sum of the mean and the standard deviation of all distances from the historical mean seasonal regime. The choice of the number of representative years, seven, was defined by the median (Stavig & Gibbons, 1977) of the number of years of all AB seasonal types. One limitation of this approach is that we cannot speak in terms of magnitude of the anomalies because of the different number of years between the seasonal types compared. Our results therefore only allow us to analyse the duration and sign of the rainfall anomalies.

3.4 | The seasonal parameters chosen to characterize different seasonal types

The onset and demise dates of the rainy season are crucial parameters for agricultural planning, for example, for determining sowing dates and whether more than one crop may be planted and harvested. In equatorial regions, for which there is no real dry season, dates delineating a wetter period were calculated.

In this study, we used the Anomalous Accumulation method developed by (Liebmann et al., 2007) which is based on a threshold easily calculable for each region because it is the daily average of the series. Since the average is recalculated for each series, and here for each

region, this method takes into account the local climatology (Arvor et al., 2014, 2017; Dubreuil et al., 2017; Liebmann et al., 2007; Michot et al.) and allows us to catch the dates of the rainy season and their shifts. The Cumulative Anomaly Method has the great advantage of systematically providing dates at the beginning and end of the rainy season or a wetter period.

An adaptation has been realized to define the onset and demise of rainfall in the seasonal types in order to take into account a shift in their dates in relation to those of the average regional regime. The deviation from the average is not calculated in relation to the daily average of their own series but in relation to that of the region. This makes it possible to identify a deviation from the average regime of the region and not simply to identify the dates corresponding to a seasonal type.

Since it is difficult to determine thresholds for rainfall quantity, the assessment of the onset and demise of the

rainiest season is estimated using pentads as in Fu et al. (2013). The dates are therefore considered early or late when the shift exceeds one pentad, that is, 5 days.

3.5 | Relationships between rainfall and oceano-atmospheric variables

Composite of seasonal anomalies of OLR and monthly anomalies IWV are the difference between the mean value of the representative years belonging to a seasonal type and the mean value of the climatological period 1981–2013 (from August year-1 to July year-0) and only the significant anomalies values (higher than 2 standard deviation; Espinoza et al., 2012; Takahashi et al., 2021) are considered. The precipitation anomalies are normalized, that is, divided by the standard deviation of the whole study period.

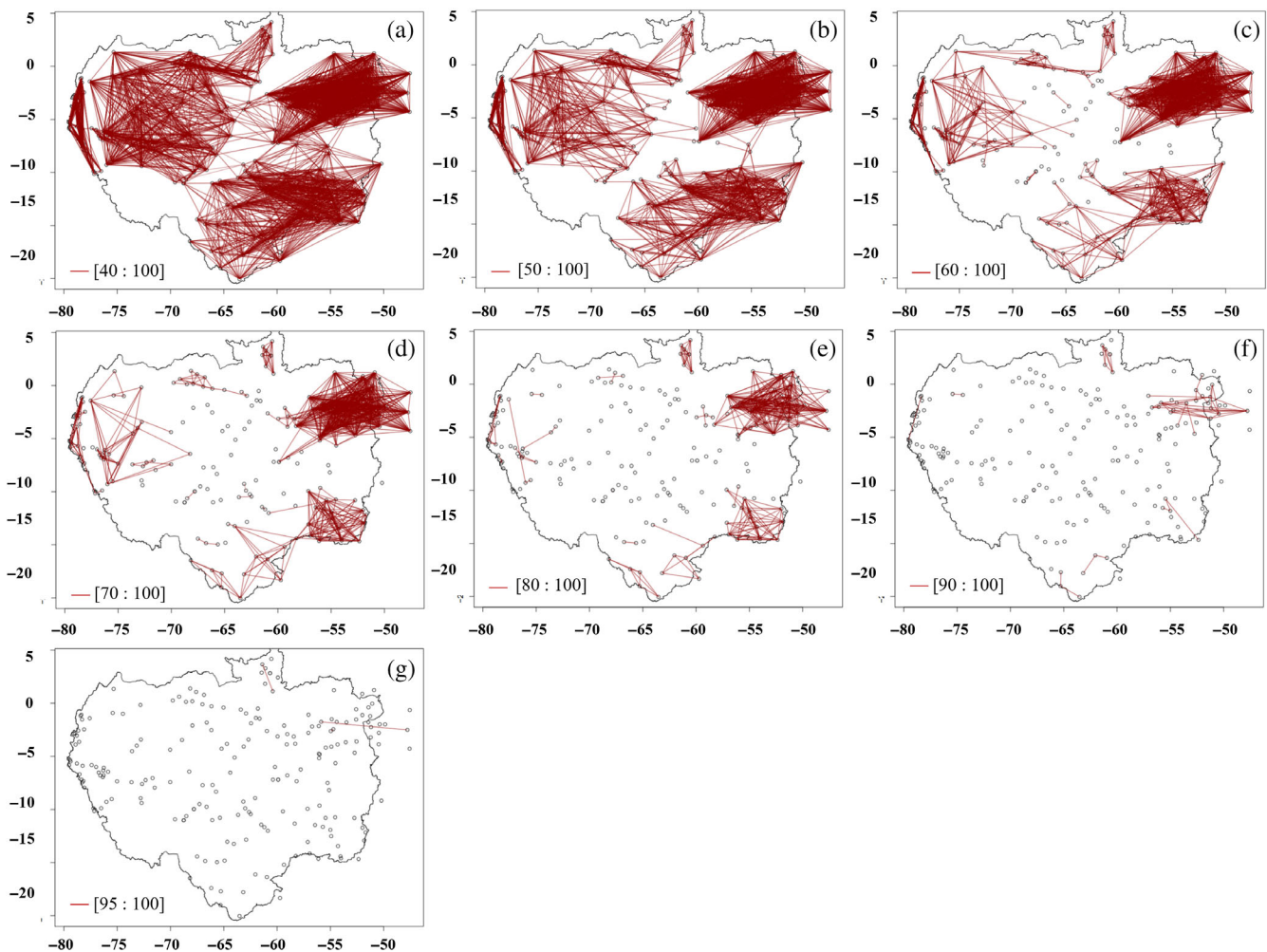


FIGURE 2 Frequency of paired stations for the period 1981–2013 at least (a) 40% of the time, (b) 50% of the time, (c) 60% of the time, (d) 70% of the time, (e) 80% of the time, (f) 90% of the time, and (g) 95% of the time. The grey dots represent the rain gauge stations, and the red lines materialize matching between two stations. [Colour figure can be viewed at wileyonlinelibrary.com]

3.6 | Homogeneous precipitation regions versus transition regions

Figure 2 shows the frequency of the annual pairing of the stations for the period 1981–2013. A spatial distinction becomes clearer when stations are paired 50% of the time (Figure 2b), that is, when they are in the same cluster half of the time. When the threshold increased to 60% (Figure 2c), there are isolated stations assigned to a transition sector as they have roughly one chance in two to belong to one group or another. Beyond a threshold of 60%, the number of linked stations falls rapidly while the number of isolated stations increases sharply. This decrease can have several explanations, including poor data coverage. Since the spatial variability of precipitation on an intra- and inter-annual scale is significant, the further apart the stations are, the less likely it is that their annual regime has been the same, and that they are

therefore grouped together several times in the same annual cluster. This explains why stations with few neighbours are linked fewer times to others and are therefore isolated. However, the northeast, north, northwest and southeast of the basin form organized groups up to a threshold of 70% (Figure 2d), indicating a greater spatial consistence of precipitation regimes in these regions. The final differentiation of the homogeneous regions results from the division of the groups of well individualized stations from there from 60%. It is important to note that these groups do not mean that all the stations are systematically linked together.

The regional classification (Figure 3) is also comparable to that provided by previous studies (Barbosa Santos et al., 2015; Delahaye et al., 2015; Espinoza Villar et al., 2009; Figueroa & Nobre, 1990). Tropical regions with dry season (northeast, north, southeast, south) are correctly distinguished from those with an equatorial

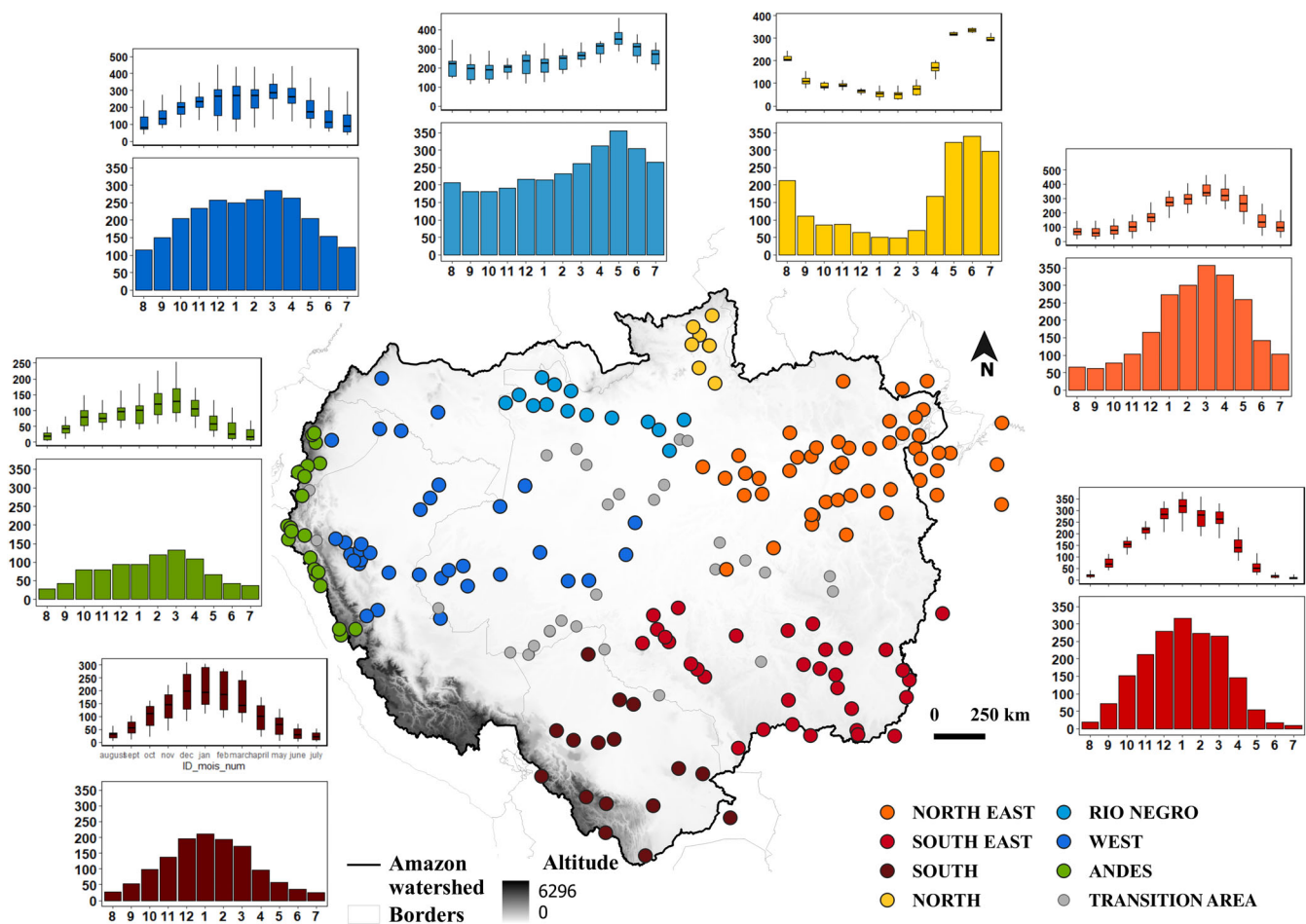


FIGURE 3 Map of homogeneous rainfall regions, with the same average rainfall regime, and transition areas (grey dots) in the Amazon basin based on spectral clustering method and results on Figure 2. The regions are formed from the stations that are grouped in at least 60% of the times in the same annual cluster (1981–2013). The graphics show per region the historical mean seasonal regime from August year-1 to July year-0 (axis x) and the monthly dispersion of the station values; the y-axis is expressed in mm. The values above the boxplots express the coefficients of variation. [Colour figure can be viewed at wileyonlinelibrary.com]

climate (without dry season; Rio Negro, western Amazon). The homogeneous climatic regions based on the cluster analysis reflects well the AB intra-seasonal spatial variability, especially between the northwest and south-east of the AB, which is coherent with the eastwards propagation of the MJO described by Mayta et al. (2019).

In more detail, a distinction among the tropical regions is well made between (i) the northeast, where the maximum rainfall is observed between March and April, during the southernmost position of the Atlantic ITCZ (Espinoza et al. 2009); (ii) the north, with a rainy season centred in the austral winter, (iii) the southeast and the south, are grouped because of their wet season in austral season but are differentiated from each other due to their different amount of rainfall. Indeed, the incursion of extra-tropical cold fronts into the Bolivian Amazon in the austral winter (Garreaud, 2000; Seluchi & Marengo, 2000), results in greater winter rainfall in the south than in the southeast (as a proportion of annual rainfall). However, in the south, the variability of precipitation between different sectors of Bolivia (Roche et al., 1990; Ronchail & Gallaire, 2006) associated with the small number of rainfall stations available for this study, leads to a fragmentation into annual clusters composed of very few stations. These were then grouped in the clusters that were spatially closest. The Andes and the Bolivian plain are thus united in the Southern region, despite the fact that rainfall variability also exists between these two sectors, as reflected in the boxplots associated with this regime in Figure 3.

In the equatorial Amazon–Andes transition zone, the stations are gathered in a single region, whereas a north-south split and a more pronounced bimodal precipitation regime would have been expected (Laraque et al., 2007; Segura et al., 2019). The unification into a single region may be related on the one hand to the fact that geographic coordinates are not taken into account in the clustering analysis (the north and south are therefore not differentiated), and the shapes of the annual distributions of the rainfall series of this region being close enough to integrate them into a common cluster. On the other hand, according to the criteria applied in our approach, the division into homogeneous regions is based on the spatial continuity of the links between the stations (Figure 2), which remains continuous at 60% and even 70%, although the links are less important between the north and the south of this Andean region. This north-south continuous homogeneity agrees with the impact of the MJO convective core propagation from the tropical Pacific to the northwestern South America, particularly identified in the Amazon–Andes transition zones of Peru and Ecuador (Recalde-Coronel et al., 2020).

The South and Andes regions have the highest heterogeneity rain gauges values as implied by the scatter

observed on the boxplots and the highest AB coefficient of variations values (Figure 3). The full diversity of local regimes, more rainfall in lowland than on the Altiplano, may not be represented; however, this more complex reality could only have been captured by creating a large number of regions. A better division of these areas could in principle be achieved using satellite products such as TRMM 3B42 version 7 (Arvor et al., 2014; Michot et al., 2018); however, a long enough (three decades) time series is not yet available.

In the northwest AB, the regimes are relatively homogeneous throughout the year; however, the distinction between the Rio Negro region and the west region is due to a different timing of the maxima, comprised between April and June for the Rio Negro region and between February and April for the western region, consistent with the quarterly rainfall percentages observed by Espinoza et al. (2009) in the basin.

It is also regrettable that no stations were available in the south–western part of the basin (between 10° S–15° S and 76° W–69° W), where it has recently been shown that the annual variability of precipitation in the southern tropical Andes is linked to a change in the dominant mode of atmospheric circulation (Segura et al., 2020). For the past 15 years, this region has been experiencing heavier precipitation between December and February, certainly due to the strengthening of the meridional circulation between the tropical North Atlantic and tropical western South America.

3.7 | Description of the seasonal types

The cluster analysis allowed to define sub-regions within the basin in which the annual rainfall cycle is spatially homogeneous. We explore now the seasonal types for each of these regions. Figure 4 shows for each region the historical mean seasonal regime (black line), the detected seasonal types (blue line), the precipitation anomalies calculated with respect to the mean seasonal regime of the region and standardized by the standard deviation of the climatology of the region (solid black) and finally, the dates of the beginning and end of the rainy season for the mean seasonal regimes (grey vertical lines) and for the seasonal types (orange vertical lines).

All regions, except the west, are characterized by four seasonal types. Some clusters include only 1 year (Figure 4b2,c1) and are thus excluded as they correspond solely to an exceptional year. Furthermore, the western region is totally excluded from the remaining of the analysis since only the anomalies of the year 1981–1982 could be distinguished in a significant way, whereas all the other years of the series are grouped in a single cluster. One of the reasons for this lower detection may be related

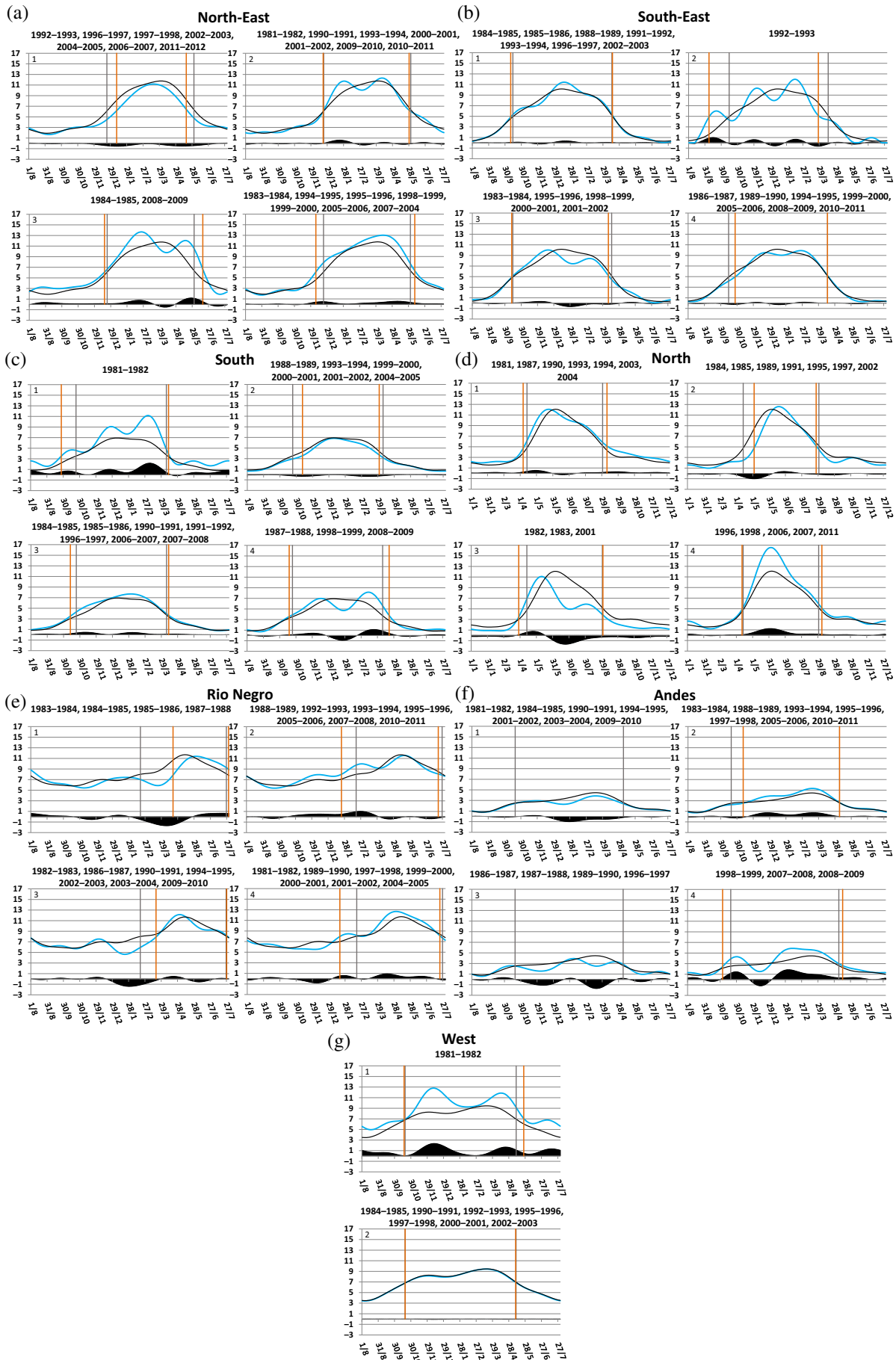


FIGURE 4 Legend on next page.

to the average regime with constant precipitation during the year and that does not vary sufficiently from a year to another to be separated by the spectral clustering method and to the exceptional 1981–1982 rainy season.

Rainy season dates are easily detected in the northeast, southeast, south and north where the seasonality is more pronounced (Figure 4a–d) and correspond to previous works (Gan et al., 2005; Kousky, 1988; Liebmann et al., 2007; Vera, Baez, et al., 2006). They are also consistent with the profile of the curves representing the seasonal types of the region. In the Rio Negro, although the regime is equatorial (no dry season), the onset of rainier periods detected in February is coherent with the seasonal regime. However, the demises in July seems to further correspond to the end of the defined hydrological year rather than a climatological feature.

In the Andes, the average onsets and demises dates define a long rainy season due to the bi-modal regime of the region. These dates are not obtained for the seasonal regime with deficient rainfall throughout the year (Figure 4f1,f3).

Table 1 summarizes the season dates (row) and the sign of the rainfall anomalies (column) of the different seasonal types. The seasonal types mainly highlight 3 kinds of rainfall anomalies (i) deficit during the whole regime, (ii) excess during the whole regime, (iii) alternating sign of the anomaly. The latter is the most frequent, corresponding to 16 out of 21 seasonal types; the rainfall anomalies often last between 30 and 60 days. It is remarkable that there are not many common years between the seasonal types of the different regions and that for the years common to the different regions, the anomalies are not the same or out of phase; there is no coherence of the seasonal types neither in time nor in space (see Figure 4). Regarding the parameters of season dates, we note that the onset of the seasonal types have higher temporal variability (later or earlier) than demise dates, particularly in the South and Rio Negro. This higher variability in the onset dates was also found by various authors (Arvor et al., 2017; Fu et al., 2013; Marengo et al., 2001; Nobre et al., 2016) for the southern Amazon region. In general, an onset shift is not necessarily associated with a demise shift. When it occurs, an early (late) onset is most often associated with a late (early) demise and therefore with a lengthening

(shortening) of the rainy season, as is the case for the seasonal type 4 in the northeast with rainfall excess during the whole regime; for type 1 in the north with alternating signs of the rainfall anomaly; for type 4 in the South with alternating signs of the anomaly and for type 4 in the Andes with alternating signs of the anomaly. On the contrary, a late onset is most often associated with an early demise and therefore with a shortening of the rainy season, as is the case for type 1 in the northeast and type 2 in the south with deficit rainfall during the whole regime for the both types. The relationship between the date of onset and the extension of the wet season agrees with the results of Fu et al. (2013) and Arvor et al. (2017) for the southern AB.

The largest shifts are detected in the Rio Negro region, with an early onset of 31 days for the seasonal type 4 and a delay of 60 days for the seasonal type 1, whereas in the southeast, although three of the four seasonal type show onset or demise shifts, the average number of days is less important. Another important information is that a type of onset and/or demise shift is not specifically associated with a particular type of rainfall anomalies during the rainy season.

These predominant rainfall anomaly features (Figure 4; Table 1) already highlight that seasonal types with alternating anomalies are marked by the superposition of intra-seasonal and inter-annual variability which are difficult to disentangle and attribute to explicit drivers with large-scale or local processes. On the contrary, the types with only excess or deficit of rainfall may be associated with large-scale and inter-annual variability drivers, for example, as a response to the inter-annual variability of SST.

4 | RELATIONSHIPS BETWEEN SEASONAL TYPES AND SST AND ATMOSPHERIC CIRCULATION

We provide a detailed observed atmospheric ocean conditions for selected seasonal types in the northeast and the southeast regions. The northeast region is strongly influenced by Pacific and Atlantic conditions (Gan et al., 2004; Liebmann & Marengo, 2001), whereas the southeast region is influenced by the South Atlantic

FIGURE 4 One to four seasonal types detected in the (a) northeast, (b) southeast, (c) south, (d) north, (e) Rio Negro, (f) Andes and (g) west regions of the Amazon basin. Years of each seasonal type are indicated above each graph. The black line represents the average precipitation regime of the region (1981–2013), the blue line the seasonal type, and solid black the precipitation anomalies (blue line minus black line). The abscissae are expressed in days of the year and the ordinates in millimetres. The dates of the onset and end of the rainy season are symbolized by the grey vertical lines for the average regime of the region, orange for the seasonal type. [Colour figure can be viewed at wileyonlinelibrary.com]

TABLE 1 Characteristics of seasonal type in the Amazon basin.

Rainy season dates		Rainfall anomaly		
		Excess all season	Deficit all season	Alternating anomalies
No rainy season dates		Andes type 2	Andes type 1	Andes type 3
Equal duration	Normal onset + normal demise			Southeast type 1 Northeast type 2
Shift season	Early onset + early demise			Southeast type 2 Rio Negro type 2
Shorter season	Normal onset + early demise			Southeast type 3
	Late onset + normal demise			North type 2 Rio Negro type 1 Rio Negro type 3 Southeast type 4
	Late onset + early demise		Northeast type 1 South type 2	
Longer season	Normal onset + late demise	North type 4		Northeast type 3
	Early onset + normal demise	South type 1 Rio Negro type 4	South type 3	North type 3
	Early onset + late demise	Northeast type 4		North type 1 South type 4 Andes type 4

Convergence Zone (SACZ), which, in turn, is partially modulated by Atlantic anomalies (Doyle & Barros, 2002; Liebmann et al., 1999; Taschetto & Wainer, 2008). In these regions, the seasonal type 1, 3 and 4 in the northeast and the seasonal type 3 in the southeast, are associated with specific sea surface temperature (SSTA) conditions.

Figure S1 in Supporting Information shows average conditions for OLR and moisture transport circulation, for easier comparison with the anomalies shown below.

4.1 | Northeast region

The northeast is the Amazon region closest to the Atlantic ocean, and there were often observed precipitation anomalies related to cloud cover, IWV and SST anomalies (Fu et al., 2001; Marengo, 2004; Tedeschi et al., 2016). Our analysis confirm that for all seasonal types a preponderant link between the ITCZ activity and position, and the precipitation in the region can be observed. For example, during December–February rainfall deficits of the seasonal type 1 (Figure 4a1) with 5 years and a late-onset season, positive OLR anomalies are observed in Figure 5i,j,k, indicating a moderate migration of the ITCZ towards the south of the tropical Atlantic and over northeastern South America. This is related to a reduction of IWV over the AB in December and January due to

weakening of the trade winds over the equatorial Atlantic, whereas the IWV east of the AB and south of south America strengthens (Figure 5i,j,k). Indeed, very heavy precipitation days (that is, daily precipitation above 20 mm) have been found to be strongly and significantly anti-correlated to the vertically integrated VIMF divergence and to the upper-level (300–100 hPa) divergence, and significantly correlated with low-level (1000–850 hPa) zonal winds in northern AB (Funatsu et al., 2021). During the second rain deficit period (March–June), the composites in Figure 5i,m–o show that OLR anomalies remain positive on the equatorial Atlantic while negative OLR anomalies are seen further north indicating few activity of the ITCZ or maybe its early northward migration. This early displacement could be due both to the strengthening of the southeasterly trade winds and weakening of the northeasterlies. In addition, divergence of the IWV from March over northeastern Brazil (Figure 5l) and from May over northern AB (Figure 5n) is observed, and the LLJ (Vera, Higgins, et al., 2006) intensified in the south. As Marengo et al. (2012) pointed out, the relative position of the ITCZ during the rainy season plays an important role on the variability of rainfall in the AB. The atmospheric anomalies are related to EN events that occur five times out of 6 years (Table 2; Figure 5a–c). These oceanic conditions alter the circulation of Walker and Hadley cells and lead to subsidence over the northeast Amazon. During the EN

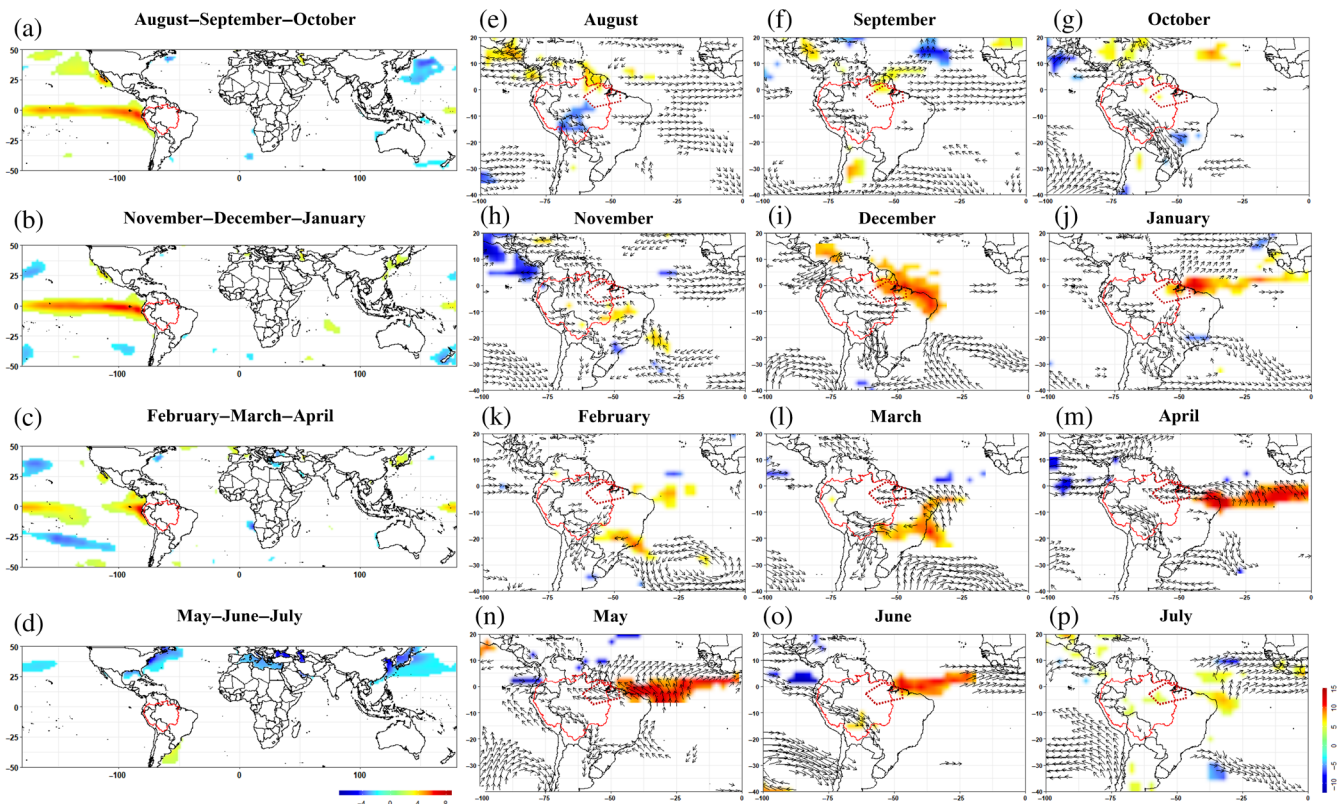


FIGURE 5 For seasonal type 1 of the northeast region (Figure 4a1), seasonal composite maps of significant anomalies from August year-1 to July year-0 of sea surface temperatures [in degree celsius; from (a) to (d)] in the left panels, and monthly composite maps of significant anomalies from August year-1 to July year-0 of outgoing longwave radiation (W/m^2) and integrated water vapour flux (vectors, in $\text{kg}\cdot\text{m}^{-1}\cdot\text{day}^{-1}$) for South America [from (e) to (p)] in the right panels. Significant anomalies are greater than 2σ . Anomalies are calculated with respect to the period 1981–2013. The red solid line represents the Amazon watershed and the red dotted line represents the northeast region. [Colour figure can be viewed at wileyonlinelibrary.com]

phase, the ITCZ is positioned further north and is less active on the AB (Hastenrath & Heller, 1977; Nobre & Moura; Nobre & Shukla, 1996).

Conversely, LN events lead to an intensification of the ascending branch of the Walker cell over the AB and promote convection (Barichivich et al., 2018; Espinoza et al., 2022; Towner et al., 2020). LN phases are related to a southward migration and more active ITCZ, driving rainfall excess on the northeast region of the AB (Marengo et al., 2012). In this study, the excess rainfall during all the year and a longer rainy season of the seasonal types 3 and 4 (Figure 4a3,a4) seem to be highly related not only to LN (Table 2) but also to north and south Atlantic anomalies. The combination of sea surface temperature anomalies, however, differs between the two seasonal type. In type 3, with 2 years, a shorter LN phase is associated with negative SSTA in the north Atlantic (NATL) and positive SSTA in the south Atlantic (SATL), whereas the LN phase of type 4 lasts longer and is only combined with positive SSTA of SATL.

In more detail, the LN phases of the seasonal type 3 are of the eastern and central type (Table 2; Andreoli

et al., 2016; Pillai et al., 2021; Tedeschi et al., 2016). Thus, the increase in cloudiness in northeastern Brazil (Figure 6i–o) is consistent with the precipitation excesses restricted to this region and observed in May by Tedeschi et al. (2016) during LN east type. According to them, the strengthening of the northeasterly trade winds and the weakening of the LLJ are more characteristic of a central LN, which is frequently related to an increased moisture convergence in the northwestern AB and to extreme floods in the Amazon River (Espinolza et al., 2014; Marengo et al., 2013). However, the negative SST in NATL (Table 2; Figure 6b,c), reinforced by the strong northerly trade winds, as well as positive SSTA in SATL (Table 2; Figure 6a; Figure S2 in Supporting Information), participate in the strong migration and maintenance southward of the ITCZ, as also observed by Wang (2004) and thus in the precipitation deficit in April then later on a late rainy season. LN and negative SSTA in the NATL leading to excess rainfall in the northeastern AB are consistent with descriptions by various authors (Hastenrath, 2001; Marengo & Hastenrath, 1993; Ronchail et al., 2002; Souza et al., 2004), but, the

TABLE 2 Synthesis of Pacific and Atlantic oceanic phases associated with northeast region seasonal types.

Seasonal types	Year	Pacific SST phase	NTATL SST phase	STATL SST phase
1: Very dry and shorter rainy season	1992–1993	Neutral	Negative	Negative
	1996–1997	Neutral	Neutral	Negative
	1997–1998	Very strong east EN	Positive	Positive
	2002–2003	Moderate central EN	Neutral	Positive
	2004–2005	Weak central EN	Positive	Positive
	2006–2007	Weak east EN	Positive	Positive
	2011–2012	Weak central LN	Neutral	Neutral
3: Contrasted anomalies and longer rainy season	1984–1985	Weak east LN	Negative	Positive
	2008–2009	Weak central LN	Neutral	Positive
4: Humid and longer rainy season	1983–1984	Weak central LN	Negative	Positive
	1994–1995	Moderate central EN	Neutral	Positive
	1995–1996	Weak east LN	Positive	Positive
	1998–1999	Strong central LN	Neutral	Positive
	1999–2000	Strong central LN	Negative	Positive
	2005–2006	Weak LN	Positive	Positive
	2007–2008	Strong LN	Neutral	Positive

Note: The central or eastern type of ENSO events is based on the classifications proposed by Andreoli et al. (2016), Pillai et al. (2021) and Tedeschi et al. (2016). Event intensity is based on the CPC–NCEP NOAA Oceanic Niño Index (ONI): weak anomaly [0.5; 0.9]; moderate anomaly [1; 1.4]; strong anomaly [1.5; 1.9]; very strong anomaly ≥ 2 . The Atlantic phases are based on the index provided by the NOAA/ESRL Physical Science Division and CIRES CU, Boulder, Colorado, from their website at <https://psl.noaa.gov/>. The phase is considered positive or negative for an anomaly beyond 0.1°C. Abbreviations: EN, El Niño; ENSO, El Niño Southern Oscillation; LN, La Niña; NCEP, National Center for Environmental Prediction; NOAA, National Ocean and Atmospheric Administration.

precipitation excesses could be further enhanced by the presence of warm SATL anomalies as observed by Nobre and Shukla (1996) and Fontaine et al. (1998). Indeed, similar to Huang and Shukla (2005), we observe that positive SATL SSTA are associated with a weakening of the sub-tropical high and associated trade winds in the South Atlantic (Figure 6i–l). Furthermore, the year of 2008–2009, which experienced exceptional flood in the AB and which is part of this seasonal type, is also described by Marengo et al. (2012) and Espinoza et al. (2022) with LN and positive SSTA in the SATL, a strong shift in the ITCZ, an intensified Walker circulation enhanced IWV from NATL, and increased precipitation in the northern and western AB.

The seasonal type 4, with 7 years, seems to be highly modulated by long LN events (Figure 7a–c) from August–1 to May, four of them being Central La Nina (Table 2). Cloudiness stretching over northeastern part of the Brazil and AB is consistent with the rainfall excesses described by Tedeschi et al. (2016) during central LN, and a stronger convergence over the northern, northeastern and central AB, while LLJ weakens (Figure 7i–l). On the contrary, positive SSTA (Table 2; Figure 7c,d; Figure S3 in Supporting Information) in the eastern equatorial Atlantic and SATL in March to May may favour convection in the ITCZ during this period and its

maintenance to the south at the end of the rainy season, as confirmed by the negative OLR anomalies. The South Atlantic SSTA, which develops more from May to July (Figure S3 in Supporting Information), can then be the cause of the resumption of rainfall at the end of the rainy season. The temporality of oceanic anomalies therefore seems to strongly modulate the temporality of precipitation.

4.2 | Southeast region

In the southeast region, seasonal type 3 (Figure 4b3) with 5 years is clearly related to the regional atmospheric circulation, and in particular the SACZ, which largely modulates the rainy season in this region. Indeed, in type 3 during the rainfall excess in October–November, negative OLR anomalies are observed over southeastern AB and Brazil, indicating the enhanced presence of the SACZ (Figure 8g,h). These excess rains are related to the decrease in IWV transport to southern South America in favour of the southeast.

Concerning Pacific SSTAs, four central LN events were present among the 5 years of this seasonal type, developing as early as August but ending early in February–April (Table 3; Figure 8a–c). Negative ENSO

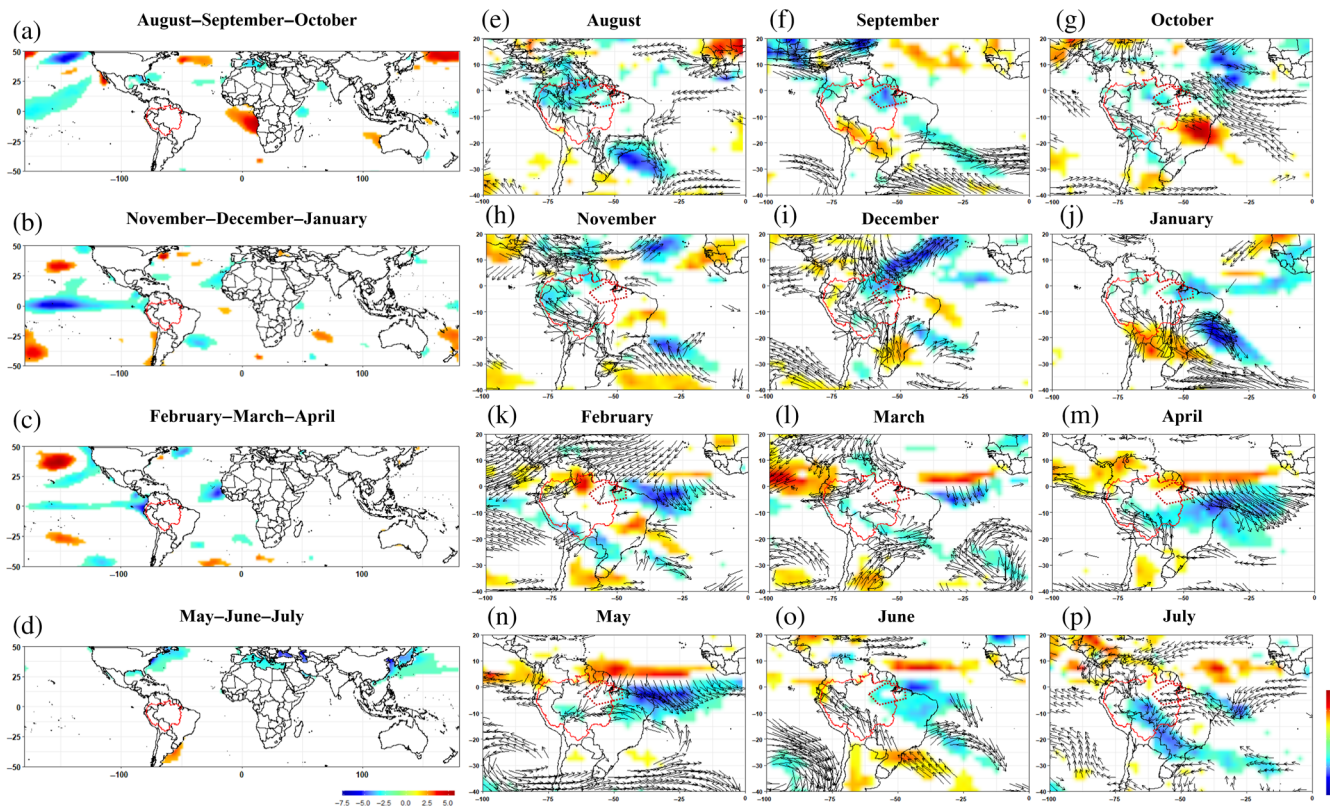


FIGURE 6 Same legend as for Figure 5, but for type 3 (Figure 4a3) in the northeast region. [Colour figure can be viewed at wileyonlinelibrary.com]

phases are known to increase convection in the AB. Here, the short period of excess rainfall and enhanced convection could correspond to the short duration of the LN events. A study by Tedeschi et al. (2016) differentiating the action of the two types of LN showed relatively low precipitation anomalies in the southern AB in both cases. Similar to Tedeschi et al. (2016), the IWV anomalies of this seasonal type have characteristics akin of that of a central LN, with convergence over the northern and northeastern AB, anti-cyclonic flux anomalies east of Brazil and convergence over the AB. However, the LN phase ends while rainfall deficits have already occurred over the region from January to April. They correspond to positive OLR anomalies (Figure 8j–m) over the extreme southeast of the AB, especially over southeastern Brazil and indicate a weak activity of the SACZ. These deficits are related to southeasterly low anomalies that partly prevent the transport of IWV from the north to the southeast region and to a weakening of the SACZ. On the contrary, the flux anomalies supplying the ITCZ move towards the eastern SATL. This configuration continues through March and persists over the southern AB into April, explaining the early demise of the rainy season (Figure 4b3). Positive SSTA near the Brazilian coast from January to April (Figure 8b,c; Figure S4 in Supporting Information) could help explain the occurrence of

these atmospheric and precipitation anomalies while the LN phase is underway. It is possible that the Atlantic SSTA reflect a weakening of the eastern branch of the South Atlantic High and thus a weakening of the easterly flux, resulting in a weakened SACZ. These observations seem to be consistent with those of Doyle and Barros (2002) who show a less active SACZ in relation to strengthened IWV towards South America and positive SSTA between 10 and 40° S, from the South American coast to 10° E. Moreover, Taschetto and Wainer (2008) indicate that the influence of the SSTA between 20 and 60° S in the Atlantic takes precedence over that of ENSO and modulates the position and intensity of the SACZ especially between December and February. Finally, positive SSTA east of SATL (Table 3; Figure 8c), from February to April, could further explain the significant activity of the ITCZ over the Atlantic, the deflection of the flux east of SATL and the early demise of the rainy season in the Southeast region.

5 | DISCUSSION AND CONCLUSION

This analysis was performed using data from 205 rain gauges, based on which the spectral clustering method

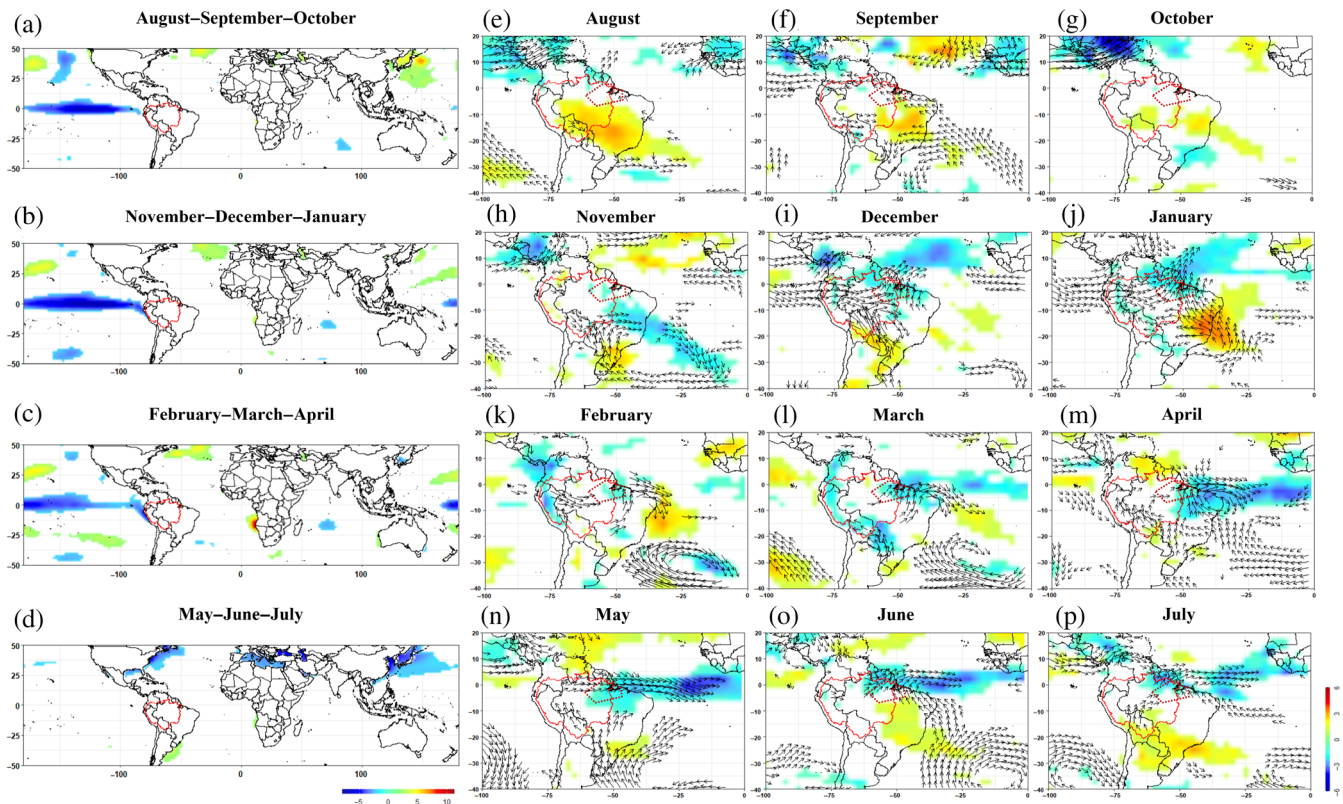


FIGURE 7 Same legend as for Figure 5, but for type 4 (Figure 4a4) in the northeast region. [Colour figure can be viewed at wileyonlinelibrary.com]

and geomatic tool allowed us to obtain seven homogeneous precipitation regions separated by transition areas, and then, within each region to detect clusters of years with similar rainfall regimes, which we referred to as seasonal types. The seven region revealed in this study show, for example, the separation between regions with or without dry seasons, between highlands and lowlands and between west and east. These regions also reflect the eastwards propagation of the MJO described by previous studies over the AB.

The seasonal types detected can be summarized by three kinds of rainfall anomalies (i) deficit during the whole year, (ii) excess during the whole year, (iii) alternating sign of the anomaly, which is the most frequent type. We found that the lag of the onset or demise rainy season dates are not associated with specific rainfall anomaly. Furthermore, the onsets of the seasonal types are more often shifted to later or earlier (than the mean average date) than demise dates, particularly in the South and Rio Negro basin (northern Amazonia). A demise shift does not appear associated with an onset shift. When it occurs, an early (late) onset is most often associated with a late (early) demise, and therefore with a lengthening (shortening) of the rainy season.

IWV and OLR anomalies are generally consistent with the rainfall anomalies characterizing each seasonal

types. In addition, in the northeast and southeast, some seasonal types are associated with SSTA in the tropical Pacific and Atlantic, that can help to understand a part of the inter-annual precipitation variability. In the northeast, as already showed in the literature, we confirmed the close relationship between precipitations anomalies and the ITCZ intensity and displacement. In this region, seasonal type corresponding to dry and shorter rainy seasons are frequently associated to EN events (mainly in central and some in the eastern Pacific), when the ITCZ moves less southwards and is less active. Conversely, longer rainy season is observed when LN events occur. However, the influence of the Atlantic SSTA is noticeable, as they also are responsible for a longer rainy season, while rainfall anomalies vary depending on timing and signal of these SSTA. When the South Atlantic SSTA are positive, rainfalls remain in excess; however, when SSTA are positive in the South Atlantic and negative on the North Atlantic, rainfall anomalies are contrasted.

In the southeast, the more relevant links between atmospheric and oceanic anomalies were observed for the seasonal types with alternating anomalies and an early demise of the rainy season. During LN conditions, we observed at the beginning of the rainy season, a more active SACZ and an excess of rainfall. During the rainy seasonal types, rainfall deficits occur when the SACZ is

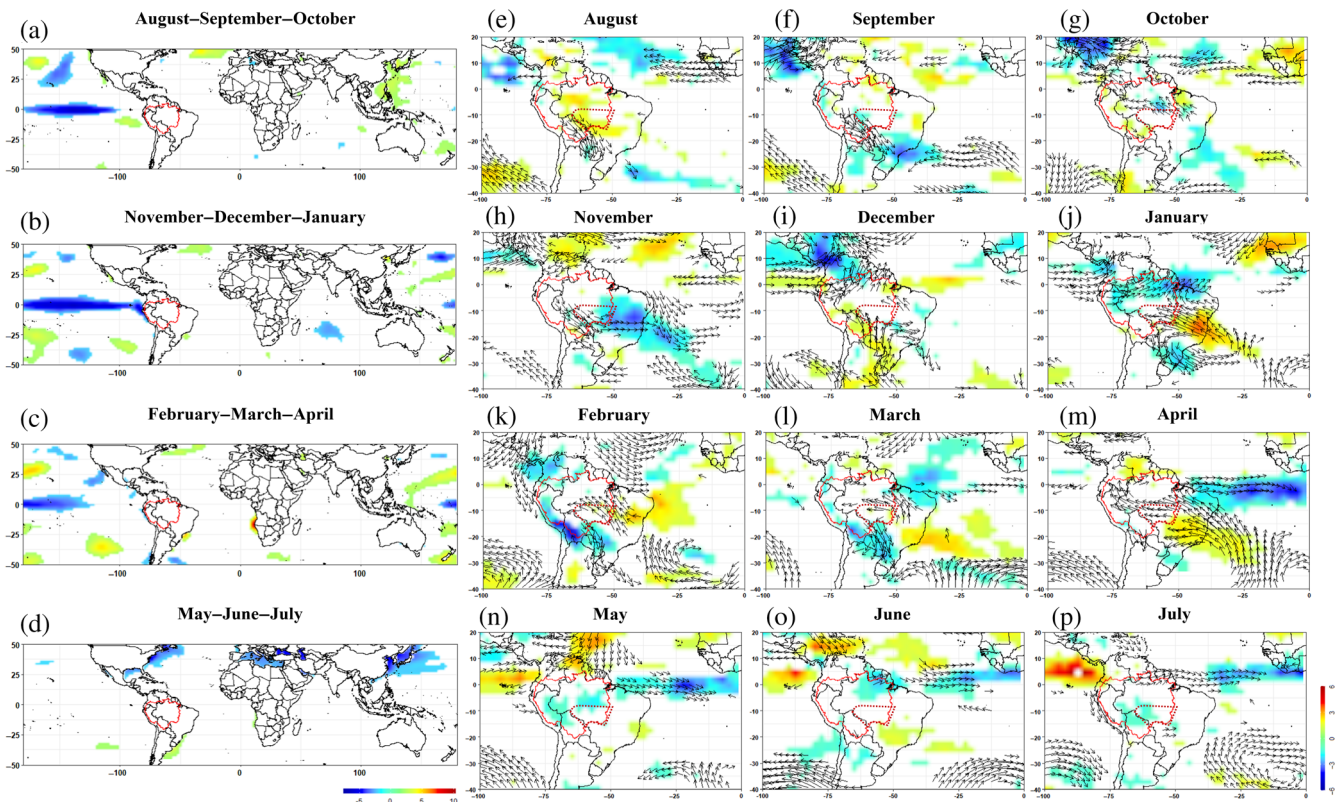


FIGURE 8 Same legend as for Figure 5, but for type 3 (Figure 4b3) in the southeast region except for the red dotted line that represents the southeast region. [Colour figure can be viewed at wileyonlinelibrary.com]

TABLE 3 Synthesis of Pacific and Atlantic oceanic phases associated with southeast region seasonal type.

Seasonal type	Year	Pacific SST phase	NATL SST phase	SATL SST phase
3: Contrasted anomalies and shorter rainy season	1983–1984	Weak central LN	Negative	Negative
	1995–1996	Weak east LN	Positive	Positive
	1998–99	Strong central LN	Neutral	Positive
	2000–2001	Weak LN	Negative	Negative
	2001–2002	Neutral	Positive	Positive

Note: The central or eastern type of ENSO events is based on the classifications proposed by Andreoli et al. (2016), Pillai et al. (2021) and Tedeschi et al. (2016). Event intensity is based on the CPC–NCEP NOAA Oceanic Niño Index (ONI): weak anomaly [0.5; 0.9]; moderate anomaly [1; 1.4]; strong anomaly [1.5; 1.9]; very strong anomaly ≥ 2 . The Atlantic phases are based on the index provided by the NOAA/ESRL Physical Science Division and CIRES CU, Boulder, Colorado, from their website at <https://psl.noaa.gov/>. The phase is considered positive or negative for an anomaly beyond 0.1°C . Abbreviations: ENSO, El Niño Southern Oscillation; NATL, specific sea surface temperature in the North Atlantic; NCEP, National Center for Environmental Prediction; NOAA, National Ocean and Atmospheric Administration; SATL, specific sea surface temperature in the South Atlantic; SST, specific sea surface.

weak because of a decrease of the IWV from the north and an anti-cyclonic anomaly of these flux in the region and southeast Brazil. These rainfall deficits and the weakening of the south Atlantic High and the SACZ could be related to positive SSTA near the Brazilian coast, which is consistent with the observations of previous studies. A relevant point to notice is that the temporality of the onset and demise of oceanic anomalies seems to strongly modulate the temporality of precipitation anomalies, as shown in previous studies (Espinoza et al. 2013; Marengo et al., 2012; Tomasella et al. 2010).

This article thus helps to summarize the diversity of regional rainy season types that can occur in Amazonia. Oceanic conditions can explain a part of the inter-annual rainfall variability; however, the superposition with intra-seasonal processes of rainfall variability remain a major issue to predict the precipitation anomalies (e.g., Mayta et al., 2019). That is why there is a need to continue to explore and understand the weight of the different factors behind these patterns of variability. First, for a better interpretation of the SSTA role on convection and IWV anomalies and on the precipitation of these seasonal

types, it will be necessary to expand the analysis using complementary variables such as vertical motions in the atmosphere and divergence/convergence fields. Furthermore, we will need to determine the drivers that influence intra-seasonal variability and in particular to investigate the role of the MJO in modulating regional rainfall anomalies for each seasonal types here. This is relevant since it is known that MJO can have significantly affect seasonal rainfall in the tropics (Zhang, 2005), especially in the SACZ area (Carvalho et al., 2004, Nogués-Paegle et al. 2000), and including extremes over the AB (Mayta et al., 2019) and tropical South America (Recalde-Coronel et al., 2020).

Our results also suggest a relevant role of local scale in modulating seasonal types. Therefore, we need to formulate some hypothesis, from land use changes (Debortoli et al., 2017; Arvor et al., 2017; Wongchuig et al., 2023., among others) to complex topography, mainly in Andean countries (Chavez & Takahashi, 2017; Espinoza et al., 2015; Junquas et al., 2018). Certainly, many other environmental parameters could contribute to influence the dates of the rainy season and rainfall anomalies (Arias et al., 2020; Fu et al., 2013; Yin et al., 2014); among them, previous dry season conditions are increasingly pointed to as factors directly influencing the mechanisms of transition to the wet season, and thus the shift in the demise of the rainy season (Marengo et al., 2022; Yin et al., 2014).

Thus, seasonal types provide an understanding of how rainfall patterns vary in the AB and are the first step in improving seasonal predictability. However, accurate prediction also depends on a good understanding of how multiscale factors modulate seasonal types which will be the subject of the next step.

AUTHOR CONTRIBUTIONS

Véronique Michot: Conceptualization; investigation; funding acquisition; writing – original draft; methodology; visualization; writing – review and editing; software; formal analysis; project administration; data curation; validation. **Thomas Corpetti:** Software; conceptualization; methodology; validation; visualization; investigation; writing – original draft. **Josyane Ronchail:** Supervision; formal analysis; writing – review and editing; funding acquisition; writing – original draft; methodology; validation; visualization; investigation; conceptualization. **Jhan Carlo Espinoza:** Formal analysis; writing – review and editing; software; visualization; validation; methodology; investigation. **Damien Arvor:** Software; visualization. **Beatriz M. Funatsu:** Writing – review and editing; visualization; validation. **Vincent Dubreuil:** Supervision; writing – review and editing; funding acquisition; writing – original draft;

methodology; validation; visualization; formal analysis; investigation; conceptualization.

ACKNOWLEDGEMENTS

The authors would like to express their thanks to the University of Rennes 2, which provided a doctoral fellowship that made this work possible, and T. Giraud from the RIATE for his precious guidelines on the use of the Cartography package. Jhan Carlo Espinoza has been supported by the French AMANECER-MOPGA project funded by ANR and IRD (ref. ANR18-MPGA-0008).

DATA AVAILABILITY STATEMENT

Data available on request from the authors.

ORCID

Véronique Michot  <https://orcid.org/0000-0001-5834-0137>

Jhan Carlo Espinoza  <https://orcid.org/0000-0001-7732-8504>

Vincent Dubreuil  <https://orcid.org/0000-0001-8383-805X>

REFERENCES

- Aceituno, P. (1988) On the functioning of the southern oscillation in the South American sector. Part I: surface climate. *Monthly Weather Review*, 116(3), 505–524. Available from: [https://doi.org/10.1175/1520-0493\(1988\)116<0505:OTFOTS>2.0.CO;2](https://doi.org/10.1175/1520-0493(1988)116<0505:OTFOTS>2.0.CO;2)
- Andreoli, R.V., de Oliveira, S.S., Kayano, M.T., Viegas, J., de Souza, R.A.F. & Candido, L.A. (2016) The influence of different El Niño types on the South American rainfall. *International Journal of Climatology*, 37, 1374–1390. Available from: <https://doi.org/10.1002/joc.4783>
- Arias, P.A., Fu, R., Vera, C. & Rojas, M. (2015) A correlated shortening of the north and south American monsoon seasons in the past few decades. *Climate Dynamics*, 45(11), 3183–3203. Available from: <https://doi.org/10.1007/s00382-015-2533-1>
- Arias, P.A., Martínez, J.A., Mejía, J.D., Pazos, M.J., Espinoza, J.C. & Wongchuig-Correa, S. (2020) Changes in normalized difference vegetation index in the Orinoco and Amazon River basins: links to tropical Atlantic surface temperatures. *Journal of Climate*, 33(19), 8537–8559. Available from: <https://doi.org/10.1175/JCLI-D-19-0696.1>
- Arraut, J.M. & Satyamurty, P. (2009) Precipitation and water vapor transport in the southern hemisphere with emphasis on the South American region. *Journal of Applied Meteorology and Climatology*, 48(9), 1902–1912. Available from: <https://doi.org/10.1175/2009jamc2030.1>
- Arvor, D., Dubreuil, V., Ronchail, J., Simões, M. & Funatsu, B.M. (2014) Spatial patterns of rainfall regimes related to levels of double cropping agriculture systems in Mato Grosso (Brazil): spatial patterns of rainfall regimes in Mato Grosso. *International Journal of Climatology*, 34(8), 2622–2633. Available from: <https://doi.org/10.1002/joc.3863>
- Arvor, D., Funatsu, B., Michot, V. & Dubreuil, V. (2017) Monitoring rainfall patterns in the southern Amazon with PERSIANN-

- CDR data: long-term characteristics and trends. *Remote Sensing*, 9(9), 889.
- Barbosa Santos, E., Sérgio Lucio, P. & Silva, C.M. (2015) Precipitation regionalization of the Brazilian Amazon. *Atmospheric Science Letters*, 16(3), 185–192.
- Barichivich, J., Gloor, E., Peylin, P., Brienen, R.J.W., Schöngart, J., Espinoza, J.C. et al. (2018) Recent intensification of Amazon flooding extremes driven by strengthened Walker circulation. *Science Advances*, 4(9), eaat8785. Available from: <https://doi.org/10.1126/sciadv.aat8785>
- Camps-Valls, G. & Bruzzone, L. (2009) *Kernel methods for remote sensing data analysis*. Natick: Wiley.
- Carvalho, L.M.V., Jones, C. & Liebmann, B. (2004) The South Atlantic convergence zone: intensity, form, persistence, and relationships with intraseasonal to interannual activity and extreme rainfall. *Journal of Climate*, 17(1), 88–108. Available from: [https://doi.org/10.1175/1520-0442\(2004\)017<0088:TSACZI>2.0.CO;2](https://doi.org/10.1175/1520-0442(2004)017<0088:TSACZI>2.0.CO;2)
- Chavez, S.P. & Takahashi, K. (2017) Orographic rainfall hot spots in the Andes-Amazon transition according to the TRMM precipitation radar and in situ data. *Journal of Geophysical Research: Atmospheres*, 122(11), 5870–5882. Available from: <https://doi.org/10.1002/2016JD026282>
- Costa, M.H. & Foley, J.A. (1998) A comparison of precipitation datasets for the Amazon basin. *Geophysical Research Letters*, 25(2), 155–158.
- Debortoli, N.S., Dubreuil, V., Hirota, M., Filho, S.R., Lindoso, D.P. & Nabucet, J. (2017) Detecting deforestation impacts in Southern Amazonia rainfall using rain gauges. *International Journal of Climatology*, 37, 2889–2900. Available from: <https://doi.org/10.1002/joc.4886>
- Delahaye, F., Kirstetter, P.E., Dubreuil, V., Machado, L.A.T., Vila, D.A. & Clark, R., III. (2015) A consistent gauge database for daily rainfall analysis over the legal Brazilian Amazon. *Journal of Hydrology*, 527, 292–304.
- Doyle, M.E. & Barros, V.R. (2002) Midsummer low-level circulation and precipitation in subtropical South America and related sea surface temperature anomalies in the South Atlantic. *Journal of Climate*, 15(23), 3394–3410. Available from: [https://doi.org/10.1175/1520-0442\(2002\)015<3394:MLLCAP>2.0.CO;2](https://doi.org/10.1175/1520-0442(2002)015<3394:MLLCAP>2.0.CO;2)
- Dubreuil, V., Funatsu, B.M., Michot, V., Nasuti, S., Debortoli, N., de Mello-Thery, N.A. et al. (2017) Local rainfall trends and their perceptions by Amazonian communities. *Climatic Change*, 143(3), 461–472. Available from: <https://doi.org/10.1007/s10584-017-2006-0>
- Durieux, L. (2002) *Etude des relations entre les caractéristiques géographiques de la surface et les nuages convectifs dans la région de l'arc de déforestation en Amazonie*. Université de Provence. UFR des sciences géographiques et de l'aménagement. <http://www.theses.fr/2002AIX10059>
- Espinoza Villar, J.C., Ronchail, J., Guyot, J.L., Cochonneau, G., Naziano, F., Lavado, W. et al. (2009) Spatio-temporal rainfall variability in the Amazon basin countries (Brazil, Peru, Bolivia, Colombia, and Ecuador). *International Journal of Climatology*, 29(11), 1574–1594.
- Espinoza Villar, J.C., Ronchail, J., Guyot, J.L., Cochonneau, G., Naziano, F., Lavado, W. et al. (2009) Spatio-temporal rainfall variability in the Amazon basin countries (Brazil, Peru, Bolivia, Colombia, and Ecuador). *International Journal of Climatology*, 29(11), 1574–1594.
- Espinoza, J.C., Marengo, J.A., Ronchail, J., Carpio, J.M., Flores, L. N. & Guyot, J.L. (2014) The extreme 2014 flood in southwestern Amazon basin: the role of tropical-subtropical South Atlantic SST gradient. *Environmental Research Letters*, 9(12), 124007. Available from: <https://doi.org/10.1088/1748-9326/9/12/124007>
- Espinoza, J.-C., Arias, P.A., Moron, V., Junquas, C., Segura, H., Sierra-Pérez, J.P. et al. (2021) Recent changes in the atmospheric circulation patterns during the dry-to-wet transition season in south tropical South America (1979–2020): impacts on precipitation and fire season. *Journal of Climate*, 34(22), 9025–9042. Available from: <https://doi.org/10.1175/JCLI-D-21-0303.1>
- Espinoza, J.-C., Marengo, J.A., Schongart, J. & Jimenez, J.C. (2022) The new historical flood of 2021 in the Amazon River compared to major floods of the 21st century: atmospheric features in the context of the intensification of floods. *Weather and Climate Extremes*, 35, 100406. Available from: <https://doi.org/10.1016/j.wace.2021.100406>
- Espinoza, J.C., Chavez, S., Ronchail, J., Junquas, C., Takahashi, K. & Lavado, W. (2015) Rainfall hotspots over the southern tropical Andes: spatial distribution, rainfall intensity, and relations with large-scale atmospheric circulation. *Water Resources Research*, 51(5), 3459–3475. Available from: <https://doi.org/10.1002/2014WR016273>
- Espinoza, J.C., Marengo, J.A., Ronchail, J., Carpio, J.M., Flores, L.N. & Guyot, J.L. (2014) The extreme 2014 flood in south-western Amazon basin: the role of tropical-subtropical South Atlantic SST gradient. *Environmental Research Letters*, 9(12), 124007. Available from: <https://doi.org/10.1088/1748-9326/9/12/124007>
- Espinoza, J.C., Ronchail, J., Frappart, F., Lavado, W., Santini, W. & Guyot, J.L. (2012) The major floods in the Amazonas River and tributaries (western Amazon Basin) during the 1970–2012 period: a focus on the 2012 flood. *Journal of Hydrometeorology*, 14(3), 1000–1008. Available from: <https://doi.org/10.1175/JHM-D-12-0100.1>
- Fassoni-Andrade, A.C., Fleischmann, A.S., Papa, F., Paiva, R.C.D., Wongchuig, S., Melack, J.M. et al. (2021) Amazon hydrology from space: scientific advances and future challenges. *Reviews of Geophysics*, 59(4), e2020RG000728. Available from: <https://doi.org/10.1029/2020RG000728>
- Figueroa, S.N. & Nobre, C.A. (1990) Precipitation distribution over central and western tropical South America. *Climanálise*, 5(6), 36–45.
- Fontaine, B., Janicot, S., Moron, V., Roucou, P. & Sylwia Trzaska, S. (1998) Anomalies de température de surface de la mer et précipitations tropicales synthèse de quelques travaux récents portant sur les précipitations au Sahel et dans le Nordeste. <http://documents.irevues.inist.fr/handle/2042/47056> [Accessed: 29th December 2016]
- Fu, R., Dickinson, R.E., Chen, M. & Wang, H. (2001) How do tropical sea surface temperatures influence the seasonal distribution of precipitation in the equatorial Amazon? *Journal of Climate*, 14(20), 4003–4026.
- Fu, R., Yin, L., Li, W., Arias, P.A., Dickinson, R.E., Huang, L. et al. (2013) Increased dry-season length over southern Amazonia in recent decades and its implication for future climate projection. *Proceedings of the National Academy of Sciences of the United States of America*, 110(45), 18110–18115.
- Funatsu, B.M., le Roux, R., Arvor, D., Espinoza, J.C., Claud, C., Ronchail, J. et al. (2021) Assessing precipitation extremes (1981–2018) and deep convective activity (2002–2018) in the Amazon region with CHIRPS and AMSU data. *Climate*

- Dynamics*, 57(3), 827–849. Available from: <https://doi.org/10.1007/s00382-021-05742-8>
- Gan, M.A., Kousky, V.E. & Ropelewski, C.F. (2004) The South America monsoon circulation and its relationship to rainfall over west-central Brazil. *Journal of Climate*, 17(1), 47–66. Available from: [https://doi.org/10.1175/1520-0442\(2004\)017<0047:TSAMCA>2.0.CO;2](https://doi.org/10.1175/1520-0442(2004)017<0047:TSAMCA>2.0.CO;2)
- Gan, M.A., Rao, V.B. & Moscati, M.C.L. (2005) South American monsoon indices. *Atmospheric Science Letters*, 6(4), 219–223. Available from: <https://doi.org/10.1002/asl.119>
- Garreaud, R. (2000) Cold air incursions over subtropical South America: mean structure and dynamics. *Monthly Weather Review*, 128(7), 2544–2559. Available from: [https://doi.org/10.1175/1520-0493\(2000\)128<2544:CAIOSS>2.0.CO;2](https://doi.org/10.1175/1520-0493(2000)128<2544:CAIOSS>2.0.CO;2)
- Hastenrath, S. (2001) In search of zonal circulations in the equatorial Atlantic sector from the NCEP–NCAR reanalysis. *International Journal of Climatology*, 21(1), 37–47.
- Hastenrath, S. & Heller, L. (1977) Dynamics of climatic hazards in northeast Brazil. *Quarterly Journal of the Royal Meteorological Society*, 103(435), 77–92.
- Huang, B. & Shukla, J. (2005) Ocean–atmosphere interactions in the tropical and subtropical Atlantic Ocean. *Journal of Climate*, 18(11), 1652–1672. Available from: <https://doi.org/10.1175/JCLI3368.1>
- Jimenez, J.C., Marengo, J.A., Alves, L.M., Sulca, J.C., Takahashi, K., Ferrett, S. et al. (2021) The role of ENSO flavours and TNA on recent droughts over Amazon forests and the northeast Brazil region. *International Journal of Climatology*, 41(7), 3761–3780. Available from: <https://doi.org/10.1002/joc.6453>
- Junquas, C., Takahashi, K., Condom, T., Espinoza, J.-C., Chavez, S., Sicart, J.-E. et al. (2018) Understanding the influence of orography on the precipitation diurnal cycle and the associated atmospheric processes in the central Andes. *Climate Dynamics*, 50(11–12), 3995–4017. Available from: <https://doi.org/10.1007/s00382-017-3858-8>
- Kalnay, E., Kanamitsu, M., Kistler, R., Collins, W., Deaven, D., Gandin, L. et al. (1996) The NCEP/NCAR 40-year reanalysis project. *Bulletin of the American Meteorological Society*, 77(3), 437–472. Available from: [https://doi.org/10.1175/1520-0477\(1996\)077<0437:TNYRP>2.0.CO;2](https://doi.org/10.1175/1520-0477(1996)077<0437:TNYRP>2.0.CO;2)
- Kousky, V.E. (1988) Pentad outgoing longwave radiation climatology for the South American sector. *Revista Brasileira de Meteorologia*, 3(1), 217–231.
- Kousky, V.E., Kagano, M.T. & Cavalcanti, I.F. (1984) A review of the southern oscillation: oceanic-atmospheric circulation changes and related rainfall anomalies. *Tellus A*, 36(5), 490–504.
- Laraque, A., Ronchail, J., Cochonneau, G., Pombosa, R. & Guyot, J.L. (2007) Heterogeneous distribution of rainfall and discharge regimes in the Ecuadorian Amazon Basin. *Journal of Hydrometeorology*, 8(6), 1364–1381.
- Liebmann, B., Camargo, S.J., Seth, A., Marengo, J.A., Carvalho, L.M.V., Allured, D. et al. (2007) Onset and end of the rainy season in South America in observations and the ECHAM 4.5 atmospheric general circulation model. *Journal of Climate*, 20(10), 2037–2050.
- Liebmann, B., Kiladis, G.N., Marengo, J.A., Ambrizzi, T. & Glick, J.D. (1999) Submonthly convective variability over South America and the South Atlantic convergence zone. *Journal of Climate*, 12(7), 1877–1891.
- Liebmann, B. & Marengo, J. (2001) Interannual variability of the rainy season and rainfall in the Brazilian Amazon Basin. *Journal of Climate*, 14(22), 4308–4318.
- Liebmann, B. & Smith, A.C. (1996) Description of a complete (interpolated) outgoing longwave radiation dataset. *Bulletin of the American Meteorological Society*, 77, 1275–1277.
- Madden, R.A. & Julian, P.R. (1971) Detection of a 40–50 day oscillation in the zonal wind in the tropical Pacific. *Journal of the Atmospheric Sciences*, 28(5), 702–708.
- Makarieva, A.M. & Gorshkov, V.G. (2007) Biotic pump of atmospheric moisture as driver of the hydrological cycle on land. *Hydrology and Earth System Sciences*, 11(2), 1013–1033. Available from: <https://doi.org/10.5194/hess-11-1013-2007>
- Marengo, J.A. (1992) Interannual variability of surface climate in the Amazon basin. *International Journal of Climatology*, 12(8), 853–863.
- Marengo, J.A. (2004) Interdecadal variability and trends of rainfall across the Amazon basin. *Theoretical and Applied Climatology*, 78(1–3), 79–96.
- Marengo, J.A., Alves, L.M., Soares, W.R., Rodriguez, D.A., Camargo, H., Riveros, M.P. et al. (2013) Two contrasting severe seasonal extremes in tropical South America in 2012: flood in Amazonia and drought in northeast Brazil. *Journal of Climate*, 26(22), 9137–9154. Available from: <https://doi.org/10.1175/JCLI-D-12-00642.1>
- Marengo, J.A., Jimenez, J.C., Espinoza, J.C., Cunha, A.P. & Aragão, L.E.O. (2022) Increased climate pressure on the agricultural frontier in the eastern Amazonia–Cerrado transition zone. *Scientific Reports*, 12(1), 457. Available from: <https://doi.org/10.1038/s41598-021-04241-4>
- Marengo, J.A., Liebmann, B., Grimm, A.M., Misra, V., Silva Dias, P.L., Cavalcanti, I.F.A. et al. (2012) Recent developments on the South American monsoon system. *International Journal of Climatology*, 32(1), 1–21. Available from: <https://doi.org/10.1002/joc.2254>
- Marengo, J.A., Liebmann, B., Kousky, V.E., Filizola, N.P. & Wainer, I.C. (2001) Onset and end of the rainy season in the Brazilian Amazon Basin. *Journal of Climate*, 14(5), 833–852. Available from: [https://doi.org/10.1175/1520-0442\(2001\)014<0833:OAEOTR>2.0.CO;2](https://doi.org/10.1175/1520-0442(2001)014<0833:OAEOTR>2.0.CO;2)
- Marengo, J.A., Nobre, C.A., Tomasella, J., Oyama, M.D., Sampaio de Oliveira, G., de Oliveira, R. et al. (2008) The drought of Amazonia in 2005. *Journal of Climate*, 21(3), 495–516.
- Marengo, J.A. & Espinoza, J.C. (2016) Extreme seasonal droughts and floods in Amazonia: causes, trends and impacts. *International Journal of Climatology*, 36(3), 1033–1050. Available from: <https://doi.org/10.1002/joc.4420>
- Marengo, J.A. & Hastenrath, S. (1993) Case studies of extreme climatic events in the Amazon Basin. *Journal of Climate*, 6(4), 617–627.
- Marques, J., Santos, J.M.D., Villa Nova, N.A. & Salati, E. (1977) Precipitable water and vapor flux between Belem and Manaus. *Acta Amazonica*, 7(3), 355–362.
- Mayta, V.C., Ambrizzi, T., Espinoza, J.C. & Silva Dias, P.L. (2019) The role of the Madden–Julian oscillation on the Amazon Basin intraseasonal rainfall variability. *International Journal of Climatology*, 39(1), 343–360. Available from: <https://doi.org/10.1002/joc.5810>
- Michot, V., Arvor, D., Ronchail, J., Corpetti, T., Jegou, N., Lucio, P.S. et al. (2019) Validation and reconstruction of rain

- gauge-based daily time series for the entire Amazon basin. *Theoretical and Applied Climatology*, 138(1), 759–775. Available from: <https://doi.org/10.1007/s00704-019-02832-w>
- Michot, V., Vila, D., Arvor, D., Corpetti, T., Ronchail, J., Funatsu, B. et al. (2018) Performance of TRMM TMPA 3B42 V7 in replicating daily rainfall and regional rainfall regimes in the Amazon Basin (1998–2013). *Remote Sensing*, 10(12), 1879. Available from: <https://doi.org/10.3390/rs10121879>
- Molion, L.C.B. (1975) *A climatonic study of the energy and moisture fluxes of the Amazonas basin with considerations of deforestation effects*. Thèse de doctorat. University of Wisconsin-Madison-Etats-Unis.
- Moron, V., Camberlin, P. & Robertson, A.W. (2013) Extracting sub-seasonal scenarios: an alternative method to analyze seasonal predictability of regional-scale tropical rainfall. *Journal of Climate*, 26(8), 2580–2600.
- Nobre, C.A., Sampaio, G., Borma, L.S., Castilla-Rubio, J.C., Silva, J.S. & Cardoso, M. (2016) Land-use and climate change risks in the Amazon and the need of a novel sustainable development paradigm. *Proceedings of the National Academy of Sciences of the United States of America*, 113(39), 10759–10768. Available from: <https://doi.org/10.1073/pnas.1605516113>
- Nobre, P. & Shukla, J. (1996) Variations of sea surface temperature, wind stress, and rainfall over the tropical Atlantic and South America. *Journal of Climate*, 9(10), 2464–2479.
- Paccini, L., Espinoza, J.C., Ronchail, J. & Segura, H. (2018) Intra-seasonal rainfall variability in the Amazon basin related to large-scale circulation patterns: a focus on western Amazon-Andes transition region: intra-seasonal rainfall variability in western Amazon. *International Journal of Climatology*, 38(5), 2386–2399. Available from: <https://doi.org/10.1002/joc.5341>
- Paegle, J.N., Byerle, L.A. & Mo, K.C. (2000) Intraseasonal modulation of South American summer precipitation. *Monthly Weather Review*, 128(3), 837–850. Available from: [https://doi.org/10.1175/1520-0493\(2000\)128<0837:imosas>2.0.co;2](https://doi.org/10.1175/1520-0493(2000)128<0837:imosas>2.0.co;2)
- Peixoto, J.P. & Oort, A.H. (1992) *Physics of climate*. New York: American Institute of Physics.
- Pillai, P.A., Ramu, D.A. & Nair, R.C. (2021) Recent changes in the major modes of Asian summer monsoon rainfall: influence of ENSO-IOD relationship. *Theoretical and Applied Climatology*, 143(3), 869–881. Available from: <https://doi.org/10.1007/s00704-020-03454-3>
- Rao, V.B. & Hada, K. (1990) Characteristics of rainfall over Brazil: annual variations and connections with the southern oscillation. *Theoretical and Applied Climatology*, 42(2), 81–91. Available from: <https://doi.org/10.1007/BF00868215>
- Recalde-Coronel, G.C., Zaitchik, B. & Pan, W.K. (2020) Madden-Julian oscillation influence on sub-seasonal rainfall variability on the west of South America. *Climate Dynamics*, 54(3), 2167–2185. Available from: <https://doi.org/10.1007/s00382-019-05107-2>
- Rocha, V.M., Correia, F.W.S. & Fonseca, P.A.M. (2015) Reciclagem de precipitação na amazônia: um estudo de revisão. *Revista Brasileira de Meteorologia*, 30(1), 59–70. Available from: <https://doi.org/10.1590/0102-778620140049>
- Roche, M.A., Aliaga, A., Campos, J., Pena, J., Cortes, J. & Rocha, N. (1990) 'Hétérogénéité des précipitations sur la cordillère des Andes boliviennes', In H. Lang & A. Musy eds. *Hydrology in Mountainous Regions. I-Hydrological Measurements; the Water Cycle*. IAHS. *International Conference on Water Resources in Mountainous Regions, Lausanne-Suisse*: International Association of Hydrological Sciences-IAHS, 381–388. Wallingford, UK: IAHS.
- Ronchail, J., Cochonneau, G., Molinier, M., Guyot, J.L., de Miranda Chaves, A.G., Guimarães, V. et al. (2002) Interannual rainfall variability in the Amazon basin and sea-surface temperatures in the equatorial Pacific and the tropical Atlantic oceans. *International Journal of Climatology*, 22(13), 1663–1686. Available from: <https://doi.org/10.1002/joc.815>
- Ronchail, J. & Gallaire, R. (2006) ENSO and rainfall along the Zongo valley (Bolivia) from the altiplano to the Amazon basin. *International Journal of Climatology*, 26(9), 1223–1236.
- Salati, E., Marques, J. & Molion, C. (1978) Origem e distribuição das chuvas na Amazônia. *Interciência*, 3(4).
- Salio, P., Nicolini, M. & Saulo, A.C. (2002) Chaco low-level jet events characterization during the austral summer season. *Journal of Geophysical Research: Atmospheres*, 107(D24), 4816.
- Satyamurty, P., da Costa, C.P.W. & Manzi, A.O. (2013) Moisture source for the Amazon basin: a study of contrasting years. *Theoretical and Applied Climatology*, 111(1), 195–209. Available from: <https://doi.org/10.1007/s00704-012-0637-7>
- Segura, H., Espinoza, J.C., Junquas, C., Lebel, T., Vuille, M. & Garreaud, R. (2020) Recent changes in the precipitation-driving processes over the southern tropical Andes/western Amazon. *Climate Dynamics*, 54(5), 2613–2631. Available from: <https://doi.org/10.1007/s00382-020-05132-6>
- Segura, H., Junquas, C., Espinoza, J.C., Vuille, M., Jauregui, Y.R., Rabatel, A. et al. (2019) New insights into the rainfall variability in the tropical Andes on seasonal and interannual time scales. *Climate Dynamics*, 53(1), 405–426. Available from: <https://doi.org/10.1007/s00382-018-4590-8>
- Seluchi, M.E. & Marengo, J.A. (2000) Tropical-midlatitude exchange of air masses during summer and winter in South America: climatic aspects and examples of intense events. *International Journal of Climatology*, 20(10), 1167–1190.
- Simões, R.M., Gan, M.A., Rocha, R.P.D. & Ambrizzi, T. (2010) Regimes de precipitação na América do Sul. *Revista Brasileira de Meteorologia*, 25(2), 185–204.
- Smith, T.M. & Reynolds, R.W. (2004) Improved extended reconstruction of SST (1854–1997). *Journal of Climate*, 17(12), 2466–2477. Available from: [https://doi.org/10.1175/1520-0442\(2004\)017<2466:IEROS>2.0.CO;2](https://doi.org/10.1175/1520-0442(2004)017<2466:IEROS>2.0.CO;2)
- Souza, E., Ambrizzi, T. & Coelho, C.A.S. (2004) Two ENSO episodes with reversed impacts on the regional precipitation of the northeastern South America. *Meteorologica*, 29(1–2), 5–16.
- Staal, A., Tuinenburg, O.A., Bosmans, J.H.C., Holmgren, M., van Nes, E.H., Scheffer, M. et al. (2018) Forest-rainfall cascades buffer against drought across the Amazon. *Nature Climate Change*, 8(6), 539–543. Available from: <https://doi.org/10.1038/s41558-018-0177-y>
- Stavig, G.R. & Gibbons, J.D. (1977) Comparing the mean and the median as measures of centrality. *International Statistical Review/Revue Internationale de Statistique*, 45(1), 63–70. Available from: <https://doi.org/10.2307/1403004>
- Sulca, J., Takahashi, K., Espinoza, J.C., Vuille, M. & Lavado-Casimiro, W. (2017) Impacts of different ENSO flavors and tropical Pacific convection variability (ITCZ, SPCZ) on austral summer rainfall in South America, with a focus on Peru.

- International Journal of Climatology*, 38, 420–435. Available from: <https://doi.org/10.1002/joc.5185>
- Takahashi, K., Montecinos, A., Goubanova, K. & Dewitte, B. (2011) ENSO regimes: reinterpreting the canonical and Modoki El Niño. *Geophysical Research Letters*, 38(10), L10704. Available from: <https://doi.org/10.1029/2011GL047364>
- Takahashi, N., Richards, K.J., Schneider, N., Annamalai, H., Hsu, W.C. & Nonaka, M. (2021) Formation mechanism of warm SST anomalies in 2010s around Hawaii. *Journal of Geophysical Research: Oceans*, 126(11), e2021JC017763. Available from: <https://doi.org/10.1029/2021JC017763>
- Taschetto, A.S. & Wainer, I. (2008) The impact of the subtropical South Atlantic SST on south American precipitation. *Annales Geophysicae*, 26(11), 3457–3476. Available from: <https://doi.org/10.5194/angeo-26-3457-2008>
- Tedeschi, R.G., Grimm, A.M. & Cavalcanti, I.F.A. (2016) Influence of central and east ENSO on precipitation and its extreme events in South America during austral autumn and winter. *International Journal of Climatology*, 36(15), 4797–4814. Available from: <https://doi.org/10.1002/joc.4670>
- Tomasella, J., Borma, L.S., Marengo, J.A., Rodriguez, D.A., Cuartas, L.A., Nobre, A. et al. (2010) The droughts of 1996–1997 and 2004–2005 in Amazonia: hydrological response in the river main-stem. *Hydrological Processes*, 25(8), 1228–1242. Portico. Available from: <https://doi.org/10.1002/hyp.7889>
- Towner, J., Cloke, H.L., Lavado, W., Santini, W., Bazo, J., Coughlan de Perez, E. et al. (2020) Attribution of Amazon floods to modes of climate variability: a review. *Meteorological Applications*, 27(5), e1949. Available from: <https://doi.org/10.1002/met.1949>
- Vera, C., Baez, J., Douglas, M., Emmanuel, C.B., Marengo, J., Meitin, J. et al. (2006) The South American low-level jet experiment. *Bulletin of the American Meteorological Society*, 87(1), 63–78. Available from: <https://doi.org/10.1175/BAMS-87-1-63>
- Vera, C., Higgins, W., Amador, J., Ambrizzi, T., Garreaud, R., Gochis, D. et al. (2006) Toward a unified view of the American monsoon systems. *Journal of Climate*, 19(20), 4977–5000. Available from: <https://doi.org/10.1175/JCLI3896.1>
- Wang, C. (2004) ENSO, Atlantic climate variability, and the Walker and Hadley circulations. In: *The Hadley circulation: present, past and future*. Dordrecht, Netherlands: Springer, pp. 173–202. Available from: http://link.springer.com/10.1007/978-1-4020-2944-8_7
- Wang, H. & Fu, R. (2002) Cross-equatorial flow and seasonal cycle of precipitation over South America. *Journal of Climate*, 15(13), 1591–1608. Available from: [https://doi.org/10.1175/1520-0442\(2002\)015<1591:CEFASC>2.0.CO;2](https://doi.org/10.1175/1520-0442(2002)015<1591:CEFASC>2.0.CO;2)
- Wongchuig, S., Carlo Espinoza, J., Condom, T., Junquas, C., Sierra, J.P., Fita, L. et al. (2023) Changes in the surface and atmospheric water budget due to projected Amazon deforestation: Lessons from a fully coupled model simulation. *Journal of Hydrology*, 625, 130082. Available from: <https://doi.org/10.1016/j.jhydrol.2023.130082>
- Yin, L., Fu, R., Zhang, Y.F., Arias, P.A., Fernando, D.N., Li, W. et al. (2014) What controls the interannual variation of the wet season onsets over the Amazon? *Journal of Geophysical Research: Atmospheres*, 119(5), 2314–2328.
- Zeng, N., Yoon, J.H., Marengo, J.A., Subramaniam, A., Nobre, C.A., Mariotti, A. et al. (2008) Causes and impacts of the 2005 Amazon drought. *Environmental Research Letters*, 3(1), 014002.
- Zhang, C. (2005) Madden-Julian Oscillation. *Reviews of Geophysics*, 43(2). Portico. Available from: <https://doi.org/10.1029/2004rg000158>
- Zubieta, R., Getirana, A., Espinoza, J.C. & Lavado, W. (2015) Impacts of satellite-based precipitation datasets on rainfall-runoff modeling of the western Amazon basin of Peru and Ecuador. *Journal of Hydrology*, 528, 599–612. Available from: <https://doi.org/10.1016/j.jhydrol.2015.06.064>
- Zulkafli, Z., Buytaert, W., Onof, C., Manz, B., Tarnavsky, E., Lavado, W. et al. (2014) A comparative performance analysis of TRMM 3B42 (TMPA) versions 6 and 7 for hydrological applications over Andean–Amazon River basins. *Journal of Hydrometeorology*, 15(2), 581–592.

SUPPORTING INFORMATION

Additional supporting information can be found online in the Supporting Information section at the end of this article.

How to cite this article: Michot, V., Corpetti, T., Ronchail, J., Espinoza, J. C., Arvor, D., Funatsu, B. M., & Dubreuil, V. (2024). Seasonal types in homogeneous rainfall regions of the Amazon basin. *International Journal of Climatology*, 1–21. <https://doi.org/10.1002/joc.8380>